An Asymptotic Analysis of Localized 3-D Spot Patterns for the Gierer-Meinhardt Model: Existence, Linear Stability and Slow Dynamics

Daniel Gomez *, Michael J. Ward †, and Juncheng Wei ‡

Abstract. Localized spot patterns, where one or more solution components concentrates at certain points in the domain, are a common class of localized pattern for reaction-diffusion systems, and they arise in a wide range of modeling scenarios. Although there is a rather well-developed theoretical understanding for this class of localized pattern in one and two space dimensions, a theoretical study of such patterns in a 3-D setting is, largely, a new frontier. In an arbitrary bounded 3-D domain, the existence, linear stability, and slow dynamics of localized multi-spot patterns is analyzed for the well-known singularly perturbed Gierer-Meinhardt (GM) activator-inhibitor system in the limit of a small activator diffusivity. Our main focus is to classify the different types of multi-spot patterns, and predict their linear stability properties, for different asymptotic ranges of the inhibitor diffusivity D. For the range $D = \mathcal{O}(\varepsilon^{-1}) \gg 1$, although both symmetric and asymmetric quasi-equilibrium spot patterns can be constructed, the asymmetric patterns are shown to be always unstable. On this range of D, it is shown that symmetric spot patterns can undergo either competition instabilities or a Hopf bifurcation, leading to spot annihilation or temporal spot amplitude oscillations, respectively. For $D = \mathcal{O}(1)$, only symmetric spot quasi-equilibria exist and they are linearly stable on $\mathcal{O}(1)$ time intervals. On this range, it is shown that the spot locations evolve slowly on an $\mathcal{O}(\varepsilon^{-3})$ time scale towards their equilibrium locations according to an ODE gradient flow, which is determined by a discrete energy involving the reduced-wave Green's function. The central role of the far-field behavior of a certain core problem, which characterizes the profile of a localized spot, for the construction of quasi-equilibria in the $D = \mathcal{O}(1)$ and $D = \mathcal{O}(\varepsilon^{-1})$ regimes, and in establishing some of their linear stability properties, is emphasized. Finally, for the range $D = \mathcal{O}(\varepsilon^2)$, it is shown that spot quasi-equilibria can undergo a peanut-splitting instability, which leads to a cascade of spot self-replication events. Predictions of the linear stability theory are all illustrated with full PDE numerical simulations of the GM model.

1. Introduction. We analyze the existence, linear stability, and slow dynamics of localized N-spot patterns for the singularly perturbed dimensionless Gierer-Meinhardt (GM) reaction-diffusion (RD) model (cf. [7])

$$v_t = \varepsilon^2 \Delta v - v + \frac{v^2}{u}\,, \quad \tau u_t = D\Delta u - u + \varepsilon^{-2} v^2\,, \quad x \in \Omega\,; \qquad \partial_n v = \partial_n u = 0\,, \quad x \in \partial\Omega\,, \tag{1.1}$$

where $\Omega \subset \mathbb{R}^3$ is a bounded domain, $\varepsilon \ll 1$, and v and u denote the activator and inhibitor fields, respectively. While the shadow limit in which $D \to \infty$ has been extensively studied (cf. [20], [22], [19]), there have relatively few studies of localized RD patterns in 3-D with a finite inhibitor diffusivity D (see [2], [5], [10], [16] and some references therein). For 3-D spot patterns, the existence, stability, and slow-dynamics of multi-spot quasi-equilibrium solutions for the singularly perturbed Schnakenberg RD model was analyzed using asymptotic methods in [16]. Although our current study is heavily influenced by [16], our results for the GM model offer some new insights into the structure of localized spot solutions for RD systems in three-dimensions. In particular, one of our key findings is the existence of two regimes, the $D = \mathcal{O}(1)$ and $D = \mathcal{O}(\varepsilon^{-1})$ regimes, for which localized patterns can be constructed in the GM-model, in contrast to the single $D = \mathcal{O}(\varepsilon^{-1})$ regime where such patterns occur for the Schnakenberg model. Furthermore, our analysis traces this distinction back to the specific far-field behaviour of the appropriate core problem,

*Dept. of Mathematics, UBC, Vancouver, Canada. (corresponding author dagubc@math.ubc.ca)
†Dept. of Mathematics, UBC, Vancouver, Canada. ward@math.ubc.ca
‡Dept. of Mathematics, UBC, Vancouver, Canada. jcwei@math.ubc.ca

characterizing the local behavior of a spot, for the GM-model. By numerically solving the core problem, we formulate a conjecture regarding the far-field limiting behavior of the solution to the core problem. With the numerically established properties of the core problem, strong localized perturbation theory (cf. [17]) is used to construct N-spot quasi-equilibrium solutions to (1.1), to study their linear stability, and to determine their slow-dynamics. We now give a more detailed outline of this paper.

In the limit $\varepsilon \to 0$, in §2 we construct N-spot quasi-equilibrium solutions to (1.1). To do so, we first formulate an appropriate core problem for a localized spot, from which we numerically compute certain key properties of its far field behavior. Using the method of matched asymptotic expansions, we then establish two distinguished regimes for the inhibitor diffusivity D, the $D = \mathcal{O}(1)$ and $D = \mathcal{O}(\varepsilon^{-1})$ regimes, for which N-spot quasi-equilibria exist. By formulating and analyzing a nonlinear algebraic system, we then demonstrate that only symmetric patterns can be constructed in the $D = \mathcal{O}(1)$ regime, whereas both symmetric and asymmetric patterns can be constructed in the $D = \mathcal{O}(\varepsilon^{-1})$ regime.

In §3 we study the linear stability on an $\mathcal{O}(1)$ time scale of the N-spot quasi-equilibria constructed in §2. More specifically, we use the method of matched asymptotic expansions to reduce a linearized eigenvalue problem to a single globally coupled eigenvalue problem. We determine that the symmetric quasi-equilibrium patterns analyzed in §2 are always linearly stable in the $D = \mathcal{O}(1)$ regime but that they may undergo both Hopf and competition instabilities in the $D = \mathcal{O}(\varepsilon^{-1})$ regime. Furthermore, we demonstrate that the asymmetric patterns studied in §2 for the $D = \mathcal{O}(\varepsilon^{-1})$ regime are always unstable. Our stability predictions are then illustrated in §5 where the finite element software FlexPDE6 [6] is used to perform full numerical simulations of (1.1) for select parameter values.

In §6 we consider the weak interaction limit, defined by $D = \mathcal{O}(\varepsilon^2)$, where localized spots interact weakly through exponentially small terms. In this regime, (1.1) can be reduced to a modified core problem from which we numerically calculate quasi-equilibria and determine their linear stability properties. Unlike in the $D = \mathcal{O}(1)$ and $D = \mathcal{O}(\varepsilon^{-1})$ regimes, we establish that spot solutions in the $D = \mathcal{O}(\varepsilon^2)$ regime can undergo *peanut-splitting* instabilities. By performing full numerical simulations using FlexPDE6 [6], we demonstrate that these instabilities lead to a cascade of spot self-replication events in 3-D. Although spike self-replication for the 1-D GM model have been studied previously in the weak interaction regime $D = \mathcal{O}(\varepsilon^2)$ (cf. [4], [8], [11]), spot self-replication for the 3-D GM model has not previously been reported.

In §7 we briefly consider the generalized GM system characterized by different exponent sets for the nonlinear kinetics. We numerically verify that the far-field behavior associated with the new core problem for the generalized GM system has the same qualitative properties as for the classical GM model (1.1) This directly implies that many of the qualitative results derived for (1.1) in §2–4 still hold in this more general setting. Finally, in §8 we summarize our findings and highlight some key open problems for future research.

2. Asymptotic Construction of an N-Spot Quasi-Equilibrium Solution.

In this section we asymptotically construct an N-spot quasi-equilibrium solution where the activator is concentrated at N specified points that are well-separated in the sense that $x_1, \ldots, x_N \in \Omega$, $|x_i - x_j| = \mathcal{O}(1)$ for $i \neq j$, and $\text{dist}(x_i, \partial\Omega) = \mathcal{O}(1)$ for $i = 1, \ldots, N$. In particular, we first outline the relevant core problem and describe some of its properties using asymptotic and numerical calculations. Then, the method of matched asymptotic expansions is used to derive a nonlinear algebraic system whose solution determines the quasi-equilibrium pattern. A key feature of this nonlinear system, in contrast to that derived in [16] for the 3-D Schnakenberg model, is is that it supports different solutions depending on whether $D = \mathcal{O}(1)$ or $D = \mathcal{O}(\varepsilon^{-1})$. More specifically, we will show that the $D = \mathcal{O}(1)$ regime admits only spot quasi-equilibria that are symmetric to leading order, whereas the $D = \mathcal{O}(\varepsilon^{-1})$ regime admits both symmetric and asym-

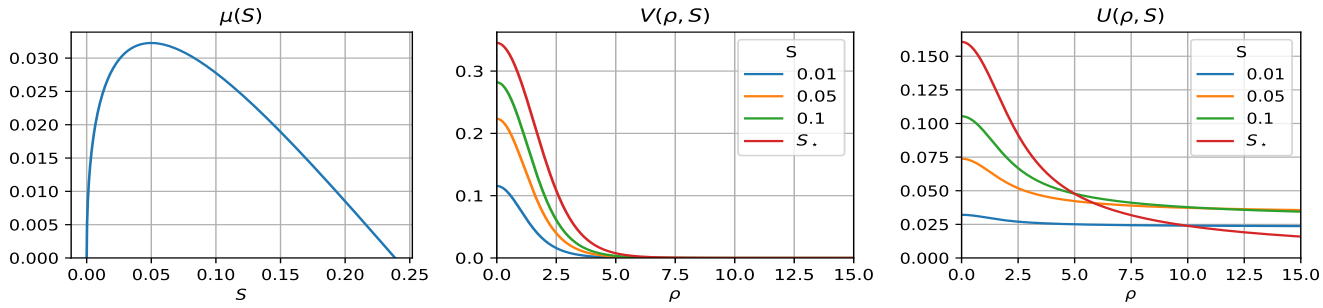

(a) (b) (c)

Figure 1: Plots of numerical solutions of the core problem (2.1): (a) $\mu(S)$ versus S, as well as the (b) activator V and (c) inhibitor U, at a few select values of S. The value $S = S_\star \approx 0.23865$ corresponds to the root of $\mu(S) = 0$.

metric N-spot quasi-equilibria.

2.1. The Core Problem. A key step in the application of the method of matched asymptotic expansions to construct localized spot patterns is the study of the core problem

$$\Delta_\rho V - V + U^{-1}V^2 = 0\,, \qquad \Delta_\rho U = -V^2\,, \qquad \rho > 0\,, \tag{2.1a}$$

$$\partial_\rho V(0) = \partial_\rho U(0) = 0\,; \qquad V \longrightarrow 0 \quad \text{and} \quad U \sim \mu(S) + S/\rho\,, \quad \rho \to \infty\,, \tag{2.1b}$$

where $\Delta_\rho \equiv \rho^{-2}\partial_\rho\left[\rho^2\partial_\rho\right]$. For a given value of $S > 0$, (2.1) is to be solved for $V = V(\rho; S)$, $U = U(\rho; S)$, and $\mu = \mu(S)$. Specifying the value of $S > 0$ is equivalent to specifying the $L^2(\mathbb{R}^3)$ norm of V, as can be verified by applying the divergence theorem to the second equation in (2.1a) over an infinitely large ball, which yields the identity $S = \int_0^\infty \rho^2\left[V(\rho)\right]^2\,d\rho$.

When $S \ll 1$ we deduce from this identity that $V = \mathcal{O}(\sqrt{S})$. By applying the divergence theorem to the first equation in (2.1a) we get $U = \mathcal{O}(\sqrt{S})$, while from (2.1b) we conclude that $\mu = \mathcal{O}(\sqrt{S})$. It is then straightforward to compute the leading order asymptotics

$$V(\rho; S) \sim \sqrt{\frac{S}{b}}w_c(\rho)\,, \qquad U(\rho; S) \sim \sqrt{\frac{S}{b}}\,, \qquad \mu(S) \sim \sqrt{\frac{S}{b}}\,, \quad \text{for} \quad S \ll 1\,, \tag{2.2}$$

where $b \equiv \int_0^\infty \rho^2\left[w_c(\rho)\right]^2\,d\rho \approx 10.423$ and $w_c > 0$ is the unique nontrivial solution to

$$\Delta_\rho w_c - w_c + w_c^2 = 0\,, \quad \rho > 0\,; \qquad \partial_\rho w_c(0) = 0\,, \qquad w_c \to 0 \quad \text{as } \rho \to \infty\,. \tag{2.3}$$

We remark that (2.3) has been well studied, with existence being proved using a constrained variational method, while its symmetry and decay properties are established by a maximum principle (see for example Appendix 13.2 of [22]). The limit case $S \ll 1$ is related to the *shadow limit* obtained by taking $D \to \infty$, for which numerous rigorous and asymptotic results have previously been obtained (cf. [20], [22], [19]).

Although the existence of solutions to (2.1) have not been rigorously established, we can use the small S asymptotics given in (2.2) as an initial guess to numerically path-follow solutions to (2.1) as S is increased. The results of our numerical computations are shown in Figure 1 where we have plotted $\mu(S)$, $V(\rho; S)$,

and $U(\rho;S)$ for select values of $S>0$. A key feature of the plot of $\mu(S)$ is that it has a zero crossing at $S=0$ and $S=S_\star\approx 0.23865$, while it attains a unique maximum on the interval $0\le S\le S_\star$ at $S=S_{\rm crit}\approx 0.04993$. Moreover, our numerical calculations indicate that $\mu''(S)<0$ on $0<S\le S_\star$. The majority of our subsequent analysis hinges on these numerically determined properties of $\mu(S)$. We leave the task of rigorously proving the existence of solutions to (2.1) and establishing the numerically verified properties of $\mu(S)$ as an open problem, which we summarize in the following conjecture:

Conjecture 2.1. *There exists a unique value of $S_\star>0$ such that (2.1) admits a ground state solution with the properties that $V,U>0$ in $\rho>0$ and for which $\mu(S_\star)=0$. Moreover, $\mu(S)$ satisfies $\mu(S)>0$ and $\mu''(S)<0$ for all $0<S<S_\star$.*

2.2. Derivation of the Nonlinear Algebraic System (NAS). We now proceed with the method of matched asymptotic expansions to construct quasi-equilibria for (1.1). First we seek an inner solution by introducing local coordinates $y=\varepsilon^{-1}(x-x_i)$ near the $i^{\rm th}$ spot and letting $v\sim DV_i(y)$ and $u\sim DU_i(y)$ so that the local steady-state problem for (1.1) becomes

$$\Delta_y V_i - V_i + U_i^{-1}V_i^2=0\,,\qquad \Delta_y U_i-\varepsilon^2 D^{-1}U_i+V_i^2=0\,,\qquad y\in\mathbb{R}^3\,. \tag{2.4}$$

In terms of the solution to the core problem (2.1) we determine that

$$V_i\sim V(\rho,S_{i\varepsilon})+\mathcal{O}(D^{-1}\varepsilon^2)\,,\qquad U_i\sim U(\rho,S_{i\varepsilon})+\mathcal{O}(D^{-1}\varepsilon^2)\,,\qquad \rho\equiv|y|=\varepsilon^{-1}|x-x_i|\,, \tag{2.5}$$

where $S_{i\varepsilon}$ is an unknown constant that depends weakly on ε. We remark that the derivation of the next order term requires that $x_1,\dots,x_N$ be allowed to vary on a slow time scale. This higher order analysis is done in §4 where we derive a system of ODE's for the spot locations.

To determine $S_{1\varepsilon},\dots,S_{N\varepsilon}$ we now derive a nonlinear algebraic system (NAS) by matching inner and outer solutions for the inhibitor field. As a first step, we calculate in the sense of distributions that $\varepsilon^{-3}v^2\longrightarrow 4\pi D^2\sum_{j=1}^N S_{j\varepsilon}\,\delta(x-x_j)+\mathcal{O}(\varepsilon^2)$ as $\varepsilon\to 0^+$. Therefore, in the outer region the inhibitor satisfies

$$\Delta u-D^{-1}u=-4\pi\varepsilon D\sum_{j=1}^N S_{j\varepsilon}\delta(x-x_j)+\mathcal{O}(\varepsilon^3)\,,\quad x\in\Omega\,;\qquad \partial_n u=0\,,\quad x\in\partial\Omega\,. \tag{2.6}$$

To solve (2.6), we let $G(x;\xi)$ denote the reduced-wave Green's function satisfying

$$\begin{aligned}&\Delta G-D^{-1}G=-\delta(x-\xi)\,,\quad x\in\Omega\,;\qquad \partial_n G=0\,,\quad x\in\partial\Omega\,,\\ &G(x;\xi)\sim\frac{1}{4\pi|x-\xi|}+R(\xi)+\nabla_x R(x;\xi)\cdot(x-\xi)\,,\qquad \text{as}\quad x\to\xi\,,\end{aligned} \tag{2.7}$$

where $R(\xi)$ is the regular part of G. The solution to (2.6) can be written as

$$u\sim 4\pi\varepsilon D\sum_{j=1}^N S_{j\varepsilon}G(x;x_j)+\mathcal{O}(\varepsilon^3)\,. \tag{2.8}$$

Before we begin matching inner and outer expansions to determine $S_{1\varepsilon},\dots,S_{N\varepsilon}$ we first motivate two distinguished limits for the relative size of D with respect to ε. To do so, we note that when $D\gg 1$ the Green's function satisfying (2.7) has the regular asymptotic expansion

$$G(x,\xi)\sim D|\Omega|^{-1}+G_0(x,\xi)+\mathcal{O}(D^{-1})\,, \tag{2.9}$$

where $G_0(x,\xi)$ is the Neumann Green's function satisfying

$$\Delta G_0 = \frac{1}{|\Omega|} - \delta(x-\xi)\,, \quad x\in\Omega\,; \qquad \partial_n G_0 = 0\,, \quad x\in\partial\Omega\,; \qquad \int_\Omega G_0\,dx = 0\,, \tag{2.10a}$$

$$G_0(x,\xi) \sim \frac{1}{4\pi|x-\xi|} + R_0(\xi) + \nabla_x R_0(x;\xi)\cdot(x-\xi)\,, \qquad \text{as} \quad x\to\xi\,, \tag{2.10b}$$

and $R_0(\xi)$ is the regular part of G_0. In summary, for the two ranges of D we have

$$G(x,\xi) \sim \frac{1}{4\pi|x-\xi|} + \begin{cases} R(\xi)+o(1)\,, & D=\mathcal{O}(1)\,,\\ D|\Omega|^{-1}+R_0(\xi)+o(1)\,, & D\gg 1\,,\end{cases} \qquad \text{as} \quad |x-\xi|\to 0\,, \tag{2.11}$$

where $R(\xi)$ is the regular part of $G(x,\xi)$. By matching the $\rho\to\infty$ behaviour of $U_i(\rho)$ given by (2.5) with the behaviour of u given by (2.8) as $|x-x_i|\to 0$, we obtain in the two regimes of D that

$$\mu(S_{i\varepsilon}) = 4\pi\varepsilon \begin{cases} S_{i\varepsilon}R(x_i) + \sum_{j\neq i} S_{j\varepsilon}G(x_i,x_j)\,, & D=\mathcal{O}(1)\,,\\ S_{i\varepsilon}R_0(x_i) + \sum_{j\neq i} S_{j\varepsilon}G_0(x_i,x_j) + D|\Omega|^{-1}\sum_{j=1}^N S_{j\varepsilon}\,, & D\gg 1\,.\end{cases} \tag{2.12}$$

¿From the $D\gg 1$ case we see that $D=\mathcal{O}(\varepsilon^{-1})$ is a distinguished regime for which the right-hand side has an $\mathcal{O}(1)$ contribution. Defining the vectors $\boldsymbol{S}_\varepsilon \equiv (S_{1\varepsilon},\ldots,S_{N\varepsilon})^T$, $\mu(\boldsymbol{S}_\varepsilon)\equiv(\mu(S_{1\varepsilon}),\ldots,\mu(S_{N\varepsilon}))^T$, and $\boldsymbol{e}\equiv(1,\ldots,1)^T$, as well as the matrices $\mathcal{E}_N$, $\mathcal{G}$, and $\mathcal{G}_0$ by

$$\mathcal{E}_N \equiv \frac{1}{N}\boldsymbol{e}\boldsymbol{e}^T\,, \qquad (\mathcal{G})_{ij} = \begin{cases} R(x_i)\,, & i=j\\ G(x_i,x_j)\,, & i\neq j\end{cases}\,, \qquad (\mathcal{G}_0)_{ij} = \begin{cases} R_0(x_i)\,, & i=j\\ G_0(x_i,x_j)\,, & i\neq j\end{cases}\,, \tag{2.13}$$

we obtain from (2.12) that the unknowns $S_{1\varepsilon},\ldots,S_{N\varepsilon}$ must satisfy the NAS

$$\mu(\boldsymbol{S}_\varepsilon) = 4\pi\varepsilon\mathcal{G}\boldsymbol{S}_\varepsilon\,, \qquad \text{for} \quad D=\mathcal{O}(1)\,, \tag{2.14a}$$

$$\mu(\boldsymbol{S}_\varepsilon) = \kappa\mathcal{E}_N\boldsymbol{S}_\varepsilon + 4\pi\varepsilon\mathcal{G}_0\boldsymbol{S}_\varepsilon\,, \qquad \text{for} \quad D=\varepsilon^{-1}D_0\,, \qquad \text{where} \quad \kappa\equiv\frac{4\pi N D_0}{|\Omega|}\,. \tag{2.14b}$$

2.3. Symmetric and Asymmetric N-Spot Quasi-Equilibrium. We now determine solutions to the NAS (2.14) in both the $D=\mathcal{O}(1)$ and the $D=\mathcal{O}(\varepsilon^{-1})$ regimes. In particular, we show that it is possible to construct *symmetric* N-spot solutions to (1.1) by finding a solution to the NAS (2.14) with $\boldsymbol{S}_\varepsilon = S_{c\varepsilon}\boldsymbol{e}$ in both the $D=\mathcal{O}(1)$ and $D=\mathcal{O}(\varepsilon^{-1})$ regimes. Moreover, when $D=\mathcal{O}(\varepsilon^{-1})$ we will show that it is possible to construct *asymmetric* quasi-equilibria to (1.1) characterized by spots each having one of two strengths.

When $D=\mathcal{O}(1)$ the NAS (2.14a) implies that to leading order $\mu(S_{i\varepsilon})=0$ for all $i=1,\ldots,N$. From the properties of $\mu(S)$ outlined in §2.1 and in particular the plot of $\mu(S)$ in Figure 1a, we deduce that $S_{i\varepsilon}\sim S_\star$ for all $i=1,\ldots,N$. Thus, to leading order, N-spot quasi-equilibria in the $D=\mathcal{O}(1)$ regime have spots with a common height, which we refer to as a *symmetric* pattern. By calculating the next order term using (2.14a) we readily obtain the two term result

$$\boldsymbol{S}_\varepsilon \sim S_\star\boldsymbol{e} + \frac{4\pi\varepsilon S_\star}{\mu'(S_\star)}\mathcal{G}\boldsymbol{e}\,. \tag{2.15}$$

We conclude that the configuration $x_1,\ldots,x_N$ of spots only affects the spot strengths at $\mathcal{O}(\varepsilon)$ through the Green's matrix $\mathcal{G}$. Note that if $\boldsymbol{e}$ is an eigenvector of $\mathcal{G}$ with eigenvalue g_0 then the solution to (2.14a) is $\boldsymbol{S}_{i\varepsilon}=S_{c\varepsilon}\boldsymbol{e}$ where $S_{c\varepsilon}$ satisfies the scalar equation $\mu(S_{c\varepsilon})=4\pi\varepsilon g_0 S_{c\varepsilon}$.

Next, we consider solutions to the NAS (2.14b) in the $D = \varepsilon^{-1} D_0$ regime. Seeking a solution $\boldsymbol{S}_\varepsilon \sim \boldsymbol{S}_0 + \varepsilon \boldsymbol{S}_1 + \cdots$ we obtain the leading order problem

$$\mu(\boldsymbol{S}_0) = \kappa \mathcal{E}_N \boldsymbol{S}_0. \tag{2.16}$$

Note that the concavity of $\mu(S)$ (see Figure 1a) implies the existence of two values $0 < S_l < S_r < S_\star$ such that $\mu(S_l) = \mu(S_r)$. Thus, in addition to the symmetric solutions already encountered in the $D = \mathcal{O}(1)$ regime, we also have the possibility of *asymmetric* solutions, where the spots can have two different heights. We first consider symmetric solutions, where to leading order $\boldsymbol{S}_0 = S_c \boldsymbol{e}$ in which S_c satisfies

$$\mu(S_c) = \kappa S_c \,. \tag{2.17}$$

The plot of $\mu(S)$ in Figure 1a, together with the $S \ll 1$ asymptotics given in (2.2), imply that a solution to (2.17) can be found in the interval $0 < S_c \leq S_\star$ for all $\kappa > 0$. In Figure 3a we illustrate graphically that the common spot strength S_c is obtained by the intersection of $\mu(S)$ with the line κS. We refer to Figure 4 for plots of the symmetric solution strengths as a function of κ. In addition, we readily calculate that

$$S_c \sim S_\star \left(1 + \frac{\kappa}{\mu'(S_\star)}\right) + \mathcal{O}(\kappa^2)\,, \quad \text{for } \kappa \ll 1\,; \qquad S_c \sim \frac{1}{b\kappa^2} + \mathcal{O}(\kappa^{-3})\,, \quad \text{for } \kappa \gg 1\,, \tag{2.18}$$

which provide a connection between the $D = \mathcal{O}(1)$ and $D \to \infty$ (shadow limit) regimes, respectively. From (2.14b), the next order correction $\boldsymbol{S}_1$ satisfies $\mu'(S_c)\boldsymbol{S}_1 - \kappa \mathcal{E}_N \boldsymbol{S}_1 = 4\pi S_c \mathcal{G}_0 \boldsymbol{e}$. Upon left-multiplying this expression by $\boldsymbol{e}^T$ we can determine $\boldsymbol{e}^T \boldsymbol{S}_1$. Then, by recalling the definition of $\mathcal{E}_N \equiv N^{-1} \boldsymbol{e}\boldsymbol{e}^T$ we can calculate $\boldsymbol{S}_1$. Summarizing, a two term asymptotic expansion for the symmetric solution to (2.14b) is

$$\boldsymbol{S}_\varepsilon \sim S_c \boldsymbol{e} + \frac{4\pi\varepsilon}{\mu'(S_c)} \left(S_c \mathcal{I}_N + \frac{\mu(S_c)}{\mu'(S_c) - \kappa} \mathcal{E}_N \right) \mathcal{G}_0 \boldsymbol{e}\,, \tag{2.19}$$

provided that $\mu'(S_c) \neq 0$ (i.e. $S_c \neq S_{\text{crit}}$). Note that $\mu'(S_c) - \kappa = 0$ is impossible by the following simple argument. First, for this equality to hold we require that $0 < S < S_{\text{crit}}$ since otherwise $\mu'(S_c) < 0$. Moreover, we can solve (2.17) for κ to get $\mu'(S_c) - \kappa = S_c^{-1} g(S_c)$ where $g(S) \equiv S\mu'(S) - \mu(S)$. However, we calculate $g'(S) = S\mu''(S) < 0$ and moreover, using the small S asymptotics found in (2.2) we determine that $g(S) \sim -\sqrt{S/(4b)} < 0$ as $S \to 0^+$. Therefore, $g(S_c) < 0$ for all $0 < S_c < S_{\text{crit}}$ so that $\mu'(S_c) < \kappa$ holds. Finally, as for the $D = \mathcal{O}(1)$ case, if $\mathcal{G}_0 \boldsymbol{e} = g_{00} \boldsymbol{e}$ then the common source values extends to higher order and we have $\boldsymbol{S}_\varepsilon = S_{c\varepsilon} \boldsymbol{e}$ where $S_{c\varepsilon}$ is the unique solution to the scalar problem

$$\mu(S_{c\varepsilon}) = (\kappa + 4\pi\varepsilon g_{00}) S_{c\varepsilon}\,. \tag{2.20}$$

Next, we construct of *asymmetric* N-spot configurations. The plot of $\mu(S)$ indicates that for any value of $S_r \in (S_{\text{crit}}, S_\star]$ there exists a unique value $S_l = S_l(S_r) \in [0, S_{\text{crit}})$ satisfying $\mu(S_l) = \mu(S_r)$. A plot of $S_l(S_r)$ is shown in Figure 2a. Clearly $S_l(S_{\text{crit}}) = S_{\text{crit}}$ and $S_l(S_\star) = 0$. We suppose that to leading order the N-spot configuration has n *large* spots of strength S_r and $N - n$ *small* spots of strengths S_l. More specifically, we seek a solution of the form

$$\boldsymbol{S}_\varepsilon \sim (S_r, \ldots, S_r, S_l(S_r), \ldots, S_l(S_r))^T\,, \tag{2.21}$$

so that (2.16) reduces to the single scalar nonlinear equation

$$\mu(S_r) = \kappa f(S_r; n/N)\,, \quad \text{on} \quad S_{\text{crit}} < S_r < S_\star\,, \qquad \text{where} \qquad f(S;\theta) \equiv \theta S + (1-\theta) S_l(S)\,. \tag{2.22}$$

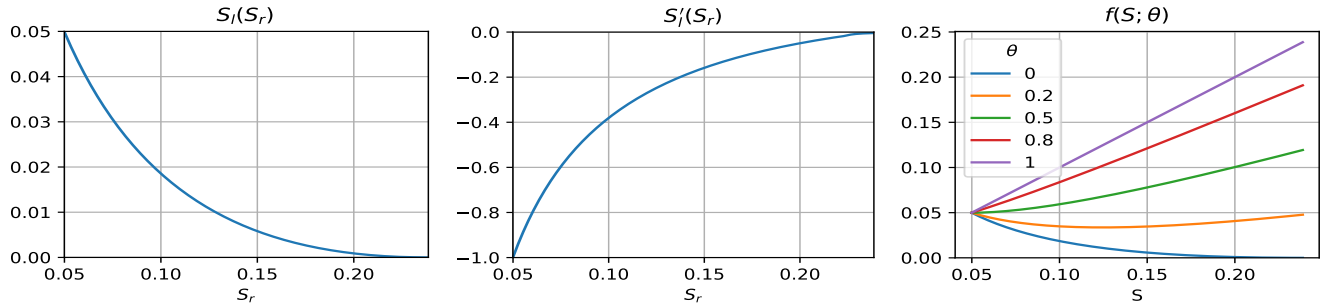

(a) (b) (c)

Figure 2: Plots of (a) $S_l(S_r)$ and (b) $S_l'(S_r)$ for the construction of asymmetric N-spot patterns. (c) Plots of $f(S,\theta)$ for select values of $\theta \equiv n/N$. For $0 < \theta < 0.5$ the function $f(S,\theta)$ attains an interior minimum in $S_{\rm crit} < S < S_\star$.

Since $\mu(S_{\rm crit}) - \kappa f(S_{\rm crit}; n/N) = \mu(S_{\rm crit}) - \kappa S_{\rm crit}$ and $\mu(S_\star) - \kappa f(S_\star; n/N) = -\kappa n S_\star/N < 0$, we obtain by the intermediate value theorem that there exists at least one solution to (2.22) for any $0 < n \leq N$ when

$$0 < \kappa < \kappa_{c1} \equiv \mu(S_{\rm crit})/S_{\rm crit} \approx 0.64619\,.$$

Next, we calculate

$$f'(S;\theta) = (1-\theta)\left(\frac{\theta}{1-\theta} + S_l'(S)\right),$$

where $S_l'(S)$ is computed numerically (see Figure 2b). We observe that $-1 \leq S_l'(S_r) \leq 0$ with $S_l'(S_{\rm crit}) = -1$ and $S_l'(S_\star) = 0$. In particular, $f(S; n/N)$ is monotone increasing if $\theta/(1-\theta) = n/(N-n) > 1$, while it attains a local minimum in $(S_{\rm crit}, S_\star)$ if $n/(N-n) < 1$. A plot of $f(S;\theta)$ is shown in Figure 2c. In either case, we deduce that the solution to (2.22) when $0 < \kappa < \kappa_{c1}$ is unique (see Figure 3a). On the other hand, when $n/(N-n) < 1$ we anticipate an additional range of values $\kappa_{c1} < \kappa < \kappa_{c2}$ for which (2.22) has *two* distinct solutions $S_{\rm crit} < \tilde{S}_r < S_r < S_\star$. Indeed, this threshold can be found by demanding that $\mu(S)$ and $\kappa f(S; n/N)$ intersect tangentially. In this way, we find that the threshold κ_{c2} can be written as

$$\kappa_{c2} = \kappa_{c2}(n/N) \equiv \frac{\mu(S_r^\star)}{f(S_r^\star; n/N)}\,, \tag{2.23a}$$

where $S_r^\star$ is the unique solution to

$$f(S_r^\star; n/N)\mu'(S_r^\star) = f'(S_r^\star; n/N)\mu(S_r^\star)\,. \tag{2.23b}$$

In Figure 3c we plot $\kappa_{c2} - \kappa_{c1}$ as a functions of n/N where we observe that $\kappa_{c2} > \kappa_{c1}$ with $\kappa_{c2} - \kappa_{c1} \to 0^+$ and $\kappa_{c2} - \kappa_{c1} \to \infty$ as $n/N \to 0.5^-$ and $n/N \to 0^+$ respectively. Furthermore, in Figure 3b we graphically illustrate how multiple solutions to (2.22) arise as $\theta = n/N$ and κ are varied. We remark that the condition $n/(N-n) < 1$ implies that $n < N/2$, so that there are more small than large spots. The appearance of two distinct asymmetric patterns in this regime has a direct analogy to results obtained for the 1-D and 2-D GM model in [18] and [21], respectively. The resulting bifurcation diagrams are shown in Figure 4 for $n/N = 0.2, 0.4, 0.6$. We summarize our results for quasi-equilibria in the following proposition.

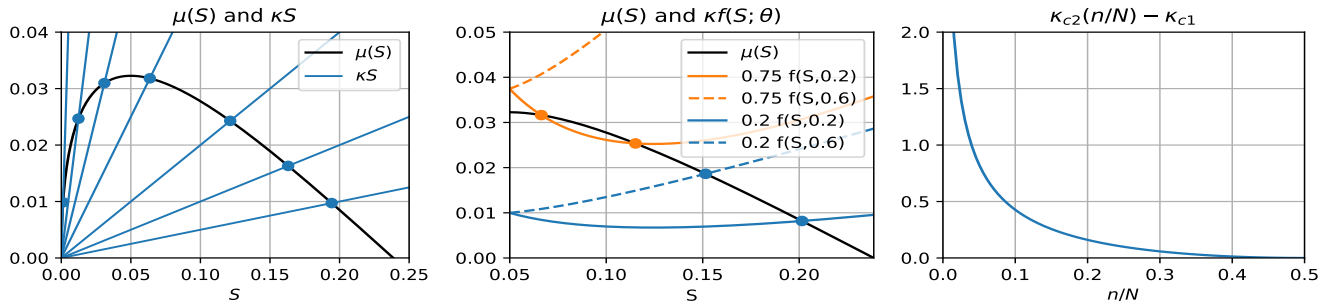

(a) (b) (c)

Figure 3: (a) Illustration of solutions to (2.17) as the intersection between $\mu(S)$ and κS. There is a unique solution if $\kappa < \kappa_{c1} \equiv \mu(S_{\rm crit})/S_{\rm crit}$. (b) Illustration of solutions to (2.22) as the intersection between $\mu(S)$ and $\kappa f(S,\theta)$ where $\theta = n/N$ denotes the fraction of *large* spots in an asymmetric pattern. Note that when $\theta = 0.2 < 0.5$ and $\kappa > \kappa_{c1} \approx 0.64619$ there exist two solutions. (c) Plot of $\kappa_{c2} - \kappa_{c1}$ versus n/N. Observe that $\kappa_{c2} - \kappa_{c1}$ increases as the fraction of large spots decreases.

Proposition 2.1. *(Quasi-Equilibria): Let $\varepsilon \to 0$ and $x_1, \ldots, x_N \in \Omega$ be well-separated. Then, the 3-D GM model (1.1) admits an N-spot quasi-equilibrium solution with inner asymptotics*

$$v \sim DV_i(\varepsilon^{-1}|x - x_i|)\,, \qquad u \sim DU_i(\varepsilon^{-1}|x - x_i|)\,, \tag{2.24}$$

as $x \to x_i$ for each $i = 1, \ldots, N$ where V_i and U_i are given by (2.5). When $|x - x_i| = \mathcal{O}(1)$, the activator is exponentially small while the inhibitor is given by (2.8). The spot strengths $S_{i\varepsilon}$ for $i = 1, \ldots, N$ completely determine the asymptotic solution and there are two distinguished limits. When $D = \mathcal{O}(1)$ the spot strengths satisfy the NAS (2.14a), which has the leading order asymptotics (2.15). In particular, $S_{i\varepsilon} \sim S_\star$ so all N-spot patterns are symmetric to leading order. When $D = \varepsilon^{-1}D_0$ the spot strengths satisfy the NAS (2.14b). A symmetric solution with asymptotics (2.19) where S_c satisfies (2.17) always exists. Moreover, if

$$0 < \frac{4\pi N D_0}{|\Omega|} < \kappa_{c1} \approx 0.64619\,,$$

then an asymmetric pattern with n large spots of strength $S_r \in (S_{crit}, S_\star)$ and $N - n$ small spots of strength $S_l \in (0, S_{crit})$ can be found by solving (2.22) for S_r and calculating S_l from $\mu(S_l) = \mu(S_r)$. If, in addition we have $n/(N-n) < 1$, then (2.22) admits two solutions on the range

$$0.64619 \approx \kappa_{c1} < \frac{4\pi N D_0}{|\Omega|} < \kappa_{c2}(n/N)\,,$$

where $\kappa_{c2}(n/N)$ is found by solving the system (2.23).

As we have already remarked, in the $D = D_0/\varepsilon$ regime, if $D_0 \ll 1$ then the symmetric N-spot solution (2.19) coincides with the symmetric solution for the $D = \mathcal{O}(1)$ regime given by (2.15). The asymmetric solutions predicted for the $D = D_0/\varepsilon$ regime persist as D_0 decreases and it is, therefore, natural to ask what these solutions correspond to in the $D = \mathcal{O}(1)$ regime. From the small S asymptotics (2.2) we note

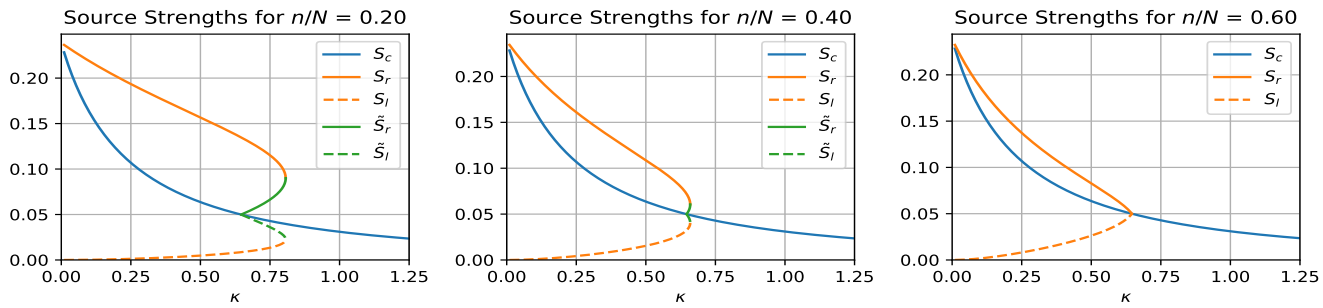

(a) (b) (c)

Figure 4: Bifurcation diagram illustrating the dependence on κ of the common spot strength S_c as well as the asymmetric spot strengths S_r and S_l or $\tilde{S}_r$ and $\tilde{S}_l$. In (a) and (b) we have $n/N < 0.5$ so that there are more small spots than large spots in an asymmetric pattern. As a result, we observe that there can be two types of asymmetric patterns with strengths S_r and S_l or $\tilde{S}_r$ and $\tilde{S}_l$. In (c) the number of large spots exceeds that of small spots and only one type of asymmetric pattern is possible.

that the NAS (2.14a) does admit an asymmetric solution, albeit one in which the source strengths of the small spots are of $\mathcal{O}(\varepsilon^2)$. Specifically, for a given integer n in $1 < n \leq N$ we can construct a solution where

$$\boldsymbol{S}_\varepsilon \sim (S_\star, \ldots, S_\star, \varepsilon^2 S_{n+1,0}, \ldots, \varepsilon^2 S_{N,0})^T . \tag{2.25}$$

By using the small S asymptotic expansion for $\mu(S)$ given in (2.2), we obtain from (2.14a) that

$$S_{i,0} = b\left(4\pi S_\star \sum_{j=1}^{n} G(x_i, x_j)\right)^2 , \qquad i = n+1, \ldots, N . \tag{2.26}$$

We observe that in order to support $N-n$ spots of strength $\mathcal{O}(\varepsilon^2)$, we require at least one spot of strength $\mathcal{O}(1)$. Setting $D = D_0/\varepsilon$, we use the large D asymptotics for $G(x,\xi)$ in (2.9) to reduce (2.26) to

$$S_{i,0} \sim b\varepsilon^{-2}\left(\frac{4\pi D_0 n S_\star}{|\Omega|}\right)^2 , \qquad i = n+1, \ldots, N . \tag{2.27}$$

Alternatively, by taking $\kappa \ll 1$ in the NAS (2.14b) for the $D = D_0/\varepsilon$ regime, we conclude that $S_r \sim S_\star$ and $S_l \sim b\,(\kappa n S_\star/N)^2$. Since $\kappa n/N = 4\pi D_0 n/|\Omega|$, as obtained from (2.14b), we confirm that the asymmetric patterns in the $D = D_0/\varepsilon$ regime lead to an asymmetric pattern consisting of spots of strength $\mathcal{O}(1)$ and $\mathcal{O}(\varepsilon^2)$ in the $D = \mathcal{O}(1)$ regime.

3. Linear Stability. Let (v_{qe}, u_{qe}) be an N-spot quasi-equilibrium solution as constructed in §2. We will analyze instabilities for quasi-equilibria that occur on $\mathcal{O}(1)$ time-scales. To do so, we substitute

$$v = v_{qe} + e^{\lambda t}\phi , \qquad u = u_{qe} + e^{\lambda t}\psi , \tag{3.1}$$

into (1.1) and, upon linearizing, we obtain the eigenvalue problem

$$\varepsilon^2\Delta\phi - \phi + \frac{2v_{qe}}{u_{qe}}\phi - \frac{v_{qe}^2}{u_{qe}^2}\psi = \lambda\phi , \qquad D\Delta\psi - \psi + 2\varepsilon^{-2}v_{qe}\phi = \tau\lambda\psi , \tag{3.2}$$

where $\partial_n\phi = \partial_n\psi = 0$ on $\partial\Omega$. In the inner region near the j^{th} spot, we introduce a local expansion in terms of the associated Legendre polynomials $P_l^m(\cos\theta)$ of degree $l = 0, 2, 3, \ldots$, and order $m = 0, 1, \ldots, l$

$$\phi \sim c_j D P_l^m(\cos\theta) e^{im\varphi}\Phi_j(\rho)\,, \qquad \psi \sim c_j D P_l^m(\cos\theta) e^{im\varphi}\Psi_j(\rho)\,, \tag{3.3}$$

where $\rho = \varepsilon^{-1}|x - x_j|$, and $(\theta, \varphi) \in (0, \pi) \times [0, 2\pi)$. Suppressing subscripts for the moment, and assuming that $\varepsilon^2\tau\lambda/D \ll 1$, we obtain the leading order inner problem

$$\Delta_\rho\Phi - \frac{l(l+1)}{\rho^2}\Phi - \Phi + \frac{2V}{U}\Phi - \frac{V^2}{U^2}\Psi = \lambda\Phi\,, \qquad \Delta_\rho\Psi - \frac{l(l+1)}{\rho^2}\Psi + 2V\Phi = 0\,, \quad \rho > 0\,, \tag{3.4a}$$

with the boundary conditions $\Phi'(0) = \Psi'(0) = 0$, and $\Phi \to 0$ as $\rho \to \infty$. Here (V, U) satisfy the core problem (2.1). The behaviour of Ψ as $\rho \to \infty$ depends on the parameter l. More specifically, we have that

$$\Psi \sim \begin{cases} B(\lambda, S) + \rho^{-1}\,, & \text{for } \ l = 0\,, \\ \rho^{-(1/2+\gamma_l)}\,, & \text{for } \ l > 0\,, \end{cases} \qquad \text{as} \quad \rho \to \infty\,, \tag{3.4b}$$

where $\gamma_l \equiv \sqrt{\frac{1}{4} + l(l+1)}$ and $B(\lambda, S)$ is a constant. Here we have normalized Ψ by fixing to unity the multiplicative factor in the decay rate in (3.4b). Next, we introduce the Green's function $G_l(\rho, \tilde\rho)$ solving

$$\Delta_\rho G_l - \frac{l(l+1)}{\rho^2}G_l = -\rho^{-2}\delta(\rho - \tilde\rho)\,, \quad \text{given by} \quad G_l(\rho, \tilde\rho) = \frac{1}{2\gamma_l\sqrt{\rho\tilde\rho}} \begin{cases} (\rho/\tilde\rho)^{\gamma_l}\,, & 0 < \rho < \tilde\rho\,, \\ (\tilde\rho/\rho)^{\gamma_l}\,, & \rho > \tilde\rho\,, \end{cases} \tag{3.5}$$

when $l > 0$. For $l = 0$ the same expression applies, but an arbitrary constant may be added. For convenience we fix this constant to be zero. In terms of this Green's function we can solve for Ψ explicitly in (3.4a) as

$$\Psi = 2\int_0^\infty G_l(\rho, \tilde\rho)V(\tilde\rho)\Phi(\tilde\rho)\tilde\rho^2\,d\tilde\rho + \begin{cases} B(\lambda, S)\,, & \text{for } \ l = 0\,, \\ 0\,, & \text{for } \ l > 0\,. \end{cases} \tag{3.6}$$

Upon substituting this expression into (3.4a) we obtain the nonlocal spectral problems

$$\mathscr{M}_0\Phi = \lambda\Phi + B(\lambda, S)\frac{V^2}{U^2}\,, \quad \text{for} \quad l = 0\,; \qquad \mathscr{M}_l\Phi = \lambda\Phi\,, \quad \text{for} \quad l > 0\,. \tag{3.7a}$$

Here the integro-differential operator $\mathscr{M}_l$ is defined for every $l \geq 0$ by

$$\mathscr{M}_l\Phi \equiv \Delta_\rho\Phi - \frac{l(l+1)}{\rho^2}\Phi - \Phi + \frac{2V}{U}\Phi - \frac{2V^2}{U^2}\int_0^\infty G_l(\rho, \tilde\rho)V(\tilde\rho)\Phi(\tilde\rho)\tilde\rho^2\,d\tilde\rho\,. \tag{3.7b}$$

A key difference between the $l = 0$ and $l > 0$ linear stability problems is the appearance of an unknown constant $B(\lambda, S)$ in the $l = 0$ equation. This unknown constant is determined by matching the far-field behaviour of the inner inhibitor expansion with the outer solution. In this sense, we expect that $B(\lambda, S)$ will encapsulate global contributions from all spots, so that instabilities for the mode $l = 0$ are due to the interactions between spots. In contrast, the absence of an unknown constant for instabilities for the $l > 0$ modes indicates that these instabilities are localized, and that the weak effect of any interactions between spots occurs only through higher order terms. In this way, instabilities for modes with $l > 0$ are determined solely by the spectrum of the operator $\mathscr{M}_l$. In Figure 5a we plot the numerically-computed

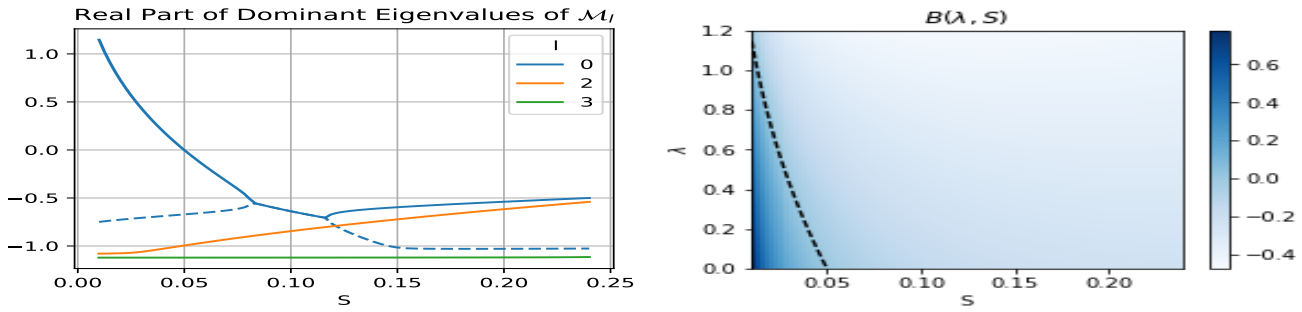

(a) (b)

Figure 5: (a) Spectrum of the operator $\mathscr{M}_l$ defined in (3.7b). The dashed blue line indicates the eigenvalue with second largest real part for $l = 0$. Notice that the dominant eigenvalue of $\mathscr{M}_0$ is zero when $S = S_{\rm crit} \approx 0.04993$, corresponding to the maximum of $\mu(S)$ (see Figure 1a). (b) Plot of $B(\lambda, S)$. The dashed line black indicates the largest positive eigenvalue of $\mathscr{M}_0(S)$ and also corresponds to the contour $B(\lambda, S) = 0$. We observe that $B(\lambda, S)$ is both continuous and negative for $S > S_{\rm crit} \approx 0.04993$.

dominant eigenvalue of $\mathscr{M}_l$ for $l = 0, 2, 3$ as well as the sub dominant eigenvalue for $l = 0$ for $0 < S < S_\star$. This spectrum is calculated from the discretization of $\mathscr{M}_l$ obtained by truncating the infinite domain to $0 < \rho < L$, with $L \gg 1$, and using a finite difference approximation for spatial derivatives combined with a trapezoidal rule discretization of the integral terms. The $l = 1$ mode always admits a zero eigenvalue, as this simply reflects the translation invariance of the inner problem. Indeed, these instabilities will be briefly considered in Section 4 where we consider the slow dynamics of quasi-equilibrium spot patterns. From Figure 5a we observe that the dominant eigenvalues of $\mathscr{M}_l$ for $l = 2, 3$ satisfy $\mathrm{Re}(\lambda) < 0$ (numerically we observe the same for larger values of l). Therefore, since the modes $l > 1$ are always *linearly stable*, for the 3-D GM model there will be no *peanut-splitting* or spot self-replication instabilities such as observed for the 3-D Schnakenberg model in [16]. In the next subsection we will focus on analyzing instabilities associated with $l = 0$ mode, which involves a global coupling between localized spots.

3.1. Competition and Hopf Instabilities for the $l = 0$ Mode. ¿From (3.7a) we observe that λ is in the spectrum of $\mathscr{M}_0$ if and only if $B(\lambda, S) = 0$. Assuming that $B(\lambda, S) \neq 0$ we can then solve for Φ in (3.7a) as

$$\Phi = B(\lambda, S)(\mathscr{M}_0 - \lambda)^{-1}(V^2/U^2)\,. \tag{3.8}$$

Upon substituting (3.8) into the expression (3.6) for Ψ when $l = 0$, we let $\rho \to \infty$ and use $G_0(\rho, \tilde{\rho}) \sim 1/\rho$ as $\rho \to \infty$, as obtained from (3.5), to deduce the far-field behavior

$$\Psi \sim B + \frac{2B}{\rho}\int_0^\infty V(\mathscr{M}_0 - \lambda)^{-1}(V^2/U^2)\rho^2 d\,\rho\,, \qquad \text{as} \quad \rho \to \infty\,. \tag{3.9}$$

We compare this expression with the normalized decay condition on Ψ in (3.4b) for $l = 0$ to conclude that

$$B(\lambda, S) = \frac{1}{2\int_0^\infty V(\mathscr{M}_0 - \lambda)^{-1}(V^2/U^2)\rho^2\, d\rho}\,. \tag{3.10}$$

We now solve the outer problem and through a matching condition derive an algebraic equation for the eigenvalue λ. Since the interaction of spots will be important for analyzing instabilities for the $l = 0$ mode,

we re-introduce the subscript j to label the spot. First, since $\partial_\rho \Psi_j \sim -\rho^{-2}$ as $\rho \to \infty$, as obtained from (3.4b) for $l = 0$, an application of the divergence theorem to $\Delta_\rho \Psi_j = -2V_j\Phi_j$ yields that $\int_0^\infty V_j \Phi_j \rho^2 \, d\rho = 1/2$. Next, by using $v_{qe} \sim DV_j(\rho)$ and $\phi \sim c_j D\Phi_j(\rho)$ for $|x - x_j| = \mathcal{O}(\varepsilon)$ as obtained from (2.24) and (3.3), respectively, we calculate in the sense of distributions for $\varepsilon \to 0$ that

$$2\varepsilon^{-2} v_{qe}\phi \to 8\pi\varepsilon D^2 \sum_{j=1}^N c_j \left(\int_0^\infty V_j \Phi_j \rho^2 \, d\rho \right) \delta(x - x_j) = 4\pi\varepsilon D^2 \sum_{j=1}^N c_j \delta(x - x_j) \, .$$

Therefore, by using this distributional limit in the equation for ψ in (3.2), the outer problem for ψ is

$$\Delta\psi - \frac{(1+\tau\lambda)}{D}\psi = -4\pi\varepsilon D \sum_{j=1}^N c_j \delta(x - x_j) \, , \quad x \in \Omega \, ; \qquad \partial_n \psi = 0 \, , \quad x \in \partial\Omega \, . \tag{3.11}$$

The solution to (3.11) is represented as

$$\psi = 4\pi\varepsilon D \sum_{j=1}^N c_j G^\lambda(x, x_j) \, , \tag{3.12}$$

where $G^\lambda(x, \xi)$ is the eigenvalue-dependent Green's function satisfying

$$\begin{aligned} &\Delta G^\lambda - \frac{(1+\tau\lambda)}{D} G^\lambda = -\delta(x - \xi) \, , \quad x \in \Omega \, ; \qquad \partial_n G^\lambda = 0 \, , \quad x \in \partial\Omega \, , \\ &G^\lambda(x, \xi) \sim \frac{1}{4\pi|x - \xi|} + R^\lambda(\xi) + o(1) \, , \qquad \text{as} \quad x \to \xi \, . \end{aligned} \tag{3.13}$$

By matching the limit as $x \to x_i$ of ψ in (3.12) with the far-field behaviour $\psi \sim Dc_i B(\lambda, S_i)$ of the inner solution, as obtained from (3.9) and (3.3), we obtain the matching condition

$$B(\lambda, S_i) c_i = 4\pi\varepsilon \left(c_i R^\lambda(x_i) + \sum_{j \neq i}^N c_j G^\lambda(x_i, x_j) \right) . \tag{3.14}$$

As similar to the construction of quasi-equilibria in §2, there are two distinguished limits $D = \mathcal{O}(1)$ and $D = D_0/\varepsilon$ to consider. The stability properties are shown to be significantly different in these two regimes.

In the $D = \mathcal{O}(1)$ regime, we recall that $S_i \sim S_\star$ for $i = 1, \ldots, N$ where $\mu(S_\star) = 0$. From (3.14), we conclude to leading order that $B(\lambda, S_\star) = 0$, so that λ must be an eigenvalue of $\mathscr{M}_0$ when $S = S_\star$. However, from Figure 5a we find that all eigenvalues of $\mathscr{M}_0$ when $S = S_\star$ satisfy $\mathrm{Re}(\lambda) < 0$. As such, from our leading order calculation we conclude that N-spot quasi-equilibria in the $D = \mathcal{O}(1)$ regime are all linearly stable.

For the remainder of this section we focus exclusively on the $D = D_0/\varepsilon$ regime. Assuming that $\varepsilon|1 + \tau\lambda|/D_0 \ll 1$ we calculate $G^\lambda(x, \xi) \sim \varepsilon^{-1} D_0 / [(1 + \tau\lambda)|\Omega|] + G_0(x, \xi)$, where G_0 is the Neumann Green's function satisfying (2.10). We substitute this limiting behavior into (3.14) and, after rewriting the the resulting homogeneous linear system for $\boldsymbol{c} \equiv (c_1, \ldots, c_N)^T$ in matrix form, we obtain

$$\mathcal{B}\boldsymbol{c} = \frac{\kappa}{1 + \tau\lambda} \mathcal{E}_N \boldsymbol{c} + 4\pi\varepsilon \mathcal{G}_0 \boldsymbol{c} \, , \qquad \text{where} \quad \mathcal{B} \equiv \mathrm{diag}(B(\lambda, S_1), \ldots, B(\lambda, S_N)) \, , \quad \mathcal{E}_N \equiv N^{-1} \boldsymbol{e}\boldsymbol{e}^T \, . \tag{3.15}$$

Here $\mathcal{G}_0$ is the Neumann Green's matrix and $\kappa \equiv 4\pi N D_0/|\Omega|$ (see (2.14b)). Next, we separate the proceeding analysis into the two cases: symmetric quasi-equilbrium patterns and asymmetric quasi-equilibria.

3.1.1. Stability of Symmetric Patterns in the $D = D_0/\varepsilon$ Regime. We suppose that the quasi-equilibrium solution is symmetric so that to leading order $S_1 = \ldots = S_N = S_c$ where S_c is found by solving the nonlinear algebraic equation (2.17). Then, from (3.15), the leading order stability problem is

$$B(\lambda, S_c)\boldsymbol{c} = \frac{\kappa}{1+\tau\lambda}\mathcal{E}_N\boldsymbol{c}\,. \tag{3.16}$$

We first consider *competition* instabilities for $N \geq 2$ characterized by $\boldsymbol{c}^T\boldsymbol{e} = 0$ so that $\mathcal{E}_N\boldsymbol{c} = 0$. Since $B(\lambda, S_c) = 0$ from (3.16), it follows that λ must be an eigenvalue of $\mathscr{M}_0$, defined in (3.7b), at $S = S_c$. From Figure 5a we deduce that the pattern is unstable for S below some threshold where the dominant eigenvalue of $\mathscr{M}_0$ equals zero. In fact, this threshold is easily determined to correspond to $S_c = S_{\rm crit}$, where $\mu'(S_{\rm crit}) = 0$, since by differentiating the core problem (2.1) with respect to S and comparing the resulting system with (3.4) when $l = 0$, we conclude that $B(0, S_c) = \mu'(S_c)$. The dotted curve in Figure 5b shows that the zero level curve $B(\lambda, S_c) = 0$ is such that $\lambda > 0$ for $S_c < S_{\rm crit}$. As such, we conclude from (2.17) that symmetric N-spot quasi-equilibria are unstable to competition instabilities when $\kappa > \kappa_{c1} \equiv \mu(S_{\rm crit})/S_{\rm crit}$.

For special spot configurations $\{x_1, \ldots, x_N\}$ where $\boldsymbol{e}$ is an eigenvector of $\mathcal{G}_0$ we can easily calculate a higher order correction to this instability threshold. Since $\mathcal{G}_0$ is symmetric, there are $N-1$ mutually orthogonal eigenvectors $\boldsymbol{q}_2, \ldots, \boldsymbol{q}_N$ such that $\mathcal{G}_0\boldsymbol{q}_k = g_k\boldsymbol{q}_k$ with $\boldsymbol{q}_k^T\boldsymbol{e} = 0$. Setting $\boldsymbol{c} = \boldsymbol{q}_k$ in (3.15), and using $B(0, S) \sim \varepsilon\mu''(S_{\rm crit})\delta$ for $S = S_{\rm crit} + \varepsilon\delta$, we can determine the perturbed stability threshold where $\lambda = 0$ associated with each eigenvector $\boldsymbol{q}_k$. By taking the minimum of such values, and by recalling the refined approximation (2.20), we obtain that N-spot symmetric quasi-equilibria are all unstable on the range

$$S_{c\varepsilon} < S_{\rm crit} + \frac{4\pi\varepsilon}{\mu''(S_{\rm crit})}\min_{k=2,\ldots,N} g_k\,. \tag{3.17}$$

Next we consider the case $\boldsymbol{c} = \boldsymbol{e}$ for which we find from (3.15) that, to leading order, λ satisfies

$$B(\lambda, S_c) - \frac{\kappa}{1+\tau\lambda} = 0\,. \tag{3.18}$$

First, we note that $\lambda = 0$ is not a solution of (3.18) since, by using $B(0, S) = \mu'(S)$, this would require that $\mu'(S_c) = \kappa$, which the short argument following (2.19) demonstrates is impossible. Therefore, the $\boldsymbol{c} = \boldsymbol{e}$ mode does not admit a zero-eigenvalue crossing and any instability that arises must occur through a Hopf bifurcation. We will seek a leading order threshold $\tau = \tau_h(\kappa)$ beyond which a Hopf bifurcation is triggered. To motivate the existence of such a threshold we consider first the $\kappa \to \infty$ limit for which the asymptotics (2.18) implies that $S_c = 1/(b\kappa^2) \ll 1$ so that from the small S expansion (2.2) of the core solution we calculate from (3.7b) that $\mathscr{M}_0\Phi \sim \Delta_\rho\Phi - \Phi + 2w_c\Phi + \mathcal{O}(\kappa^{-1})$. Then, by substituting this expression, together with the small S asymptotics (2.2) where $S_c \sim 1/b\kappa^2 \ll 1$, into (3.10) we can determine $B(\lambda, S_c)$ when $\kappa \gg 1$. Then, by using the resulting expression for B in (3.18), we obtain the following well-known nonlocal eigenvalue problem (NLEP) corresponding to the shadow limit $\kappa = 4\pi N D_0/|\Omega| \to \infty$:

$$1 + \tau\lambda - \frac{2\int_0^\infty w_c(\Delta_\rho - 1 + 2w_c - \lambda)^{-1}w_c^2\rho^2\,d\rho}{\int_0^\infty w_c^2\rho^2\,d\rho} = 0\,. \tag{3.19}$$

¿From Table 1 in [19], this NLEP has a Hopf bifurcation at $\tau = \tau_h^\infty \approx 0.373$ with corresponding critical eigenvalue $\lambda = i\lambda_h^\infty$ with $\lambda_h^\infty \approx 2.174$. To determine $\tau_h(\kappa)$ for $\kappa = \mathcal{O}(1)$, we set $\lambda = i\lambda_h$ in (3.18) and separate the resulting expression into real and imaginary parts to obtain

$$\tau_h = -\frac{\mathrm{Im}\left(B(i\lambda_h, S_c)\right)}{\lambda_h \mathrm{Re}\left(B(i\lambda_h, S_c)\right)}\,, \qquad \frac{|B(i\lambda_h, S_c)|^2}{\mathrm{Re}\left(B(i\lambda_h, S_c)\right)} - \kappa = 0\,, \tag{3.20}$$

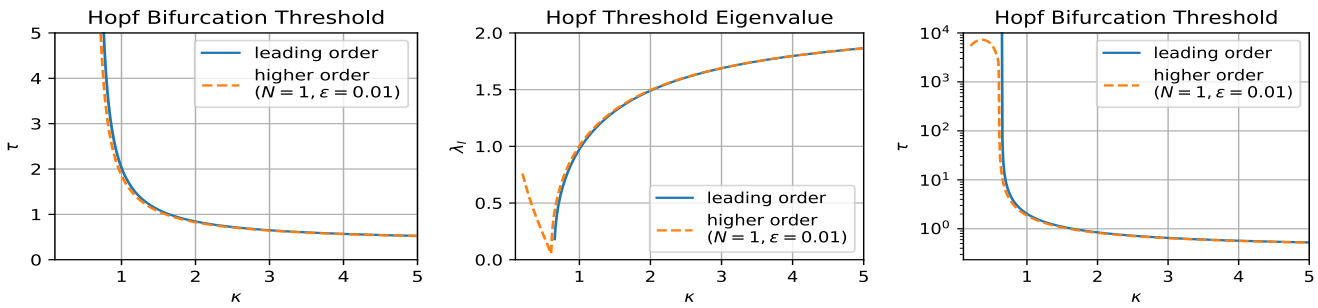

(a) (b) (c)

Figure 6: Leading order (a) Hopf bifurcation threshold $\tau_h(\kappa)$ and (b) critical eigenvalue $\lambda = i\lambda_h$ for a symmetric N-spot pattern as calculated by solving (3.20) numerically. The leading order theory assumes $\varepsilon|1+\tau\lambda|/D_0 \ll 1$ and is independent of the spot locations. We calculate the higher order Hopf bifurcation threshold for an $N = 1$ spot pattern centered at the origin of the unit ball with $\varepsilon = 0.01$ by solving (3.14) directly (note $\kappa = 3D_0$). In (c) we see that although the leading order Hopf bifurcation threshold diverges as $\kappa \to \kappa_{c1}$, going to higher order demonstrates that a large but finite threshold persists.

where S_c depends on κ from (2.17). Starting with $\kappa = 50$ we solve the second equation for λ_h using Newton's method with $\lambda_h = \lambda_h^\infty$ as an initial guess. We then use the first equation to calculate τ_h. Decreasing κ and using the previous solution as an initial guess we obtain the curves $\tau_h(\kappa)$ and $\lambda_h(\kappa)$ as shown in Figure 6.

We conclude this section by noting that as seen in Figures 6a and 6c the leading order Hopf bifurcation threshold diverges as $\kappa \to \kappa_{c1}^+$, where $\kappa_{c1} = \mu(S_{\rm crit})/S_{\rm crit}$. This is a direct consequence of the assumption that $\varepsilon|1+\tau\lambda|/D_0 \ll 1$ which fails to hold as τ gets increasingly large. Indeed, by using the series expansion in (3.12)–(3.14) of [12] for the reduced wave Green's function in the sphere, we can solve (3.14) directly using Newton's method for an $N = 1$ spot configuration centered at the origin of the unit ball. Fixing $\varepsilon = 0.001$, this yields the higher order asymptotic approximation for the Hopf bifurcation threshold indicated by the dashed lines in Figure 6. This shows that to higher order the bifurcation threshold is large but finite in the region $\kappa \le \kappa_{c1}$. Moreover, it hints at an ε dependent rescaling of τ in the region $\kappa \le \kappa_{c1}$ for which a counterpart to (3.16) may be derived. While we do not undertake this rescaling in this paper we remark that for 2-D spot patterns this rescaling led to the discovery in [15] of an *anomalous* scaling law for the Hopf threshold.

3.1.2. Stability of Asymmetric Patterns in the $D = D_0/\varepsilon$ Regime. When the N-spot pattern consists of n *large* spots of strength $S_1 = \ldots = S_n = S_r$ and $N - n$ *small* spots of strength $S_{n+1} = \ldots = S_N = S_l$, the leading order linear stability is characterized by the blocked matrix system

$$\begin{pmatrix} B(\lambda, S_r)\mathcal{I}_n & 0 \\ 0 & B(\lambda, S_l)\mathcal{I}_{N-n} \end{pmatrix} \boldsymbol{c} = \frac{\kappa}{1+\tau\lambda}\mathcal{E}_N \boldsymbol{c}\,, \tag{3.21}$$

where $\mathcal{I}_m$ denotes the $m \times m$ identity matrix. In particular, an asymmetric quasi-equilibrium solution is linearly unstable if this system admits any nontrivial modes, $\boldsymbol{c}$, for which λ has a positive real part. We will show that asymmetric patterns are always unstable by explicitly constructing unstable modes.

First, we assume that $1 \le n < N-1$ and we choose $\boldsymbol{c}$ to be a mode satisfying

$$c_1 = \cdots = c_n = 0\,, \qquad c_{n+1} + \cdots + c_N = 0\,. \tag{3.22}$$

Note that this mode describes *competition* among the $N-n$ small spots of strength S_l. For such a mode, (3.21) reduces to the single equation $B(\lambda, S_l) = 0$, which implies that λ must be an eigenvalue of $\mathcal{M}_0$ at $S = S_l$. However, since $S_l < S_{\rm crit}$, we deduce from Figure 5a that there exists a real and positive λ for $\mathcal{M}_0$ at $S = S_l$. As such, any mode $\boldsymbol{c}$ satisfying (3.22) is linearly unstable.

We must consider the $n = N-1$ case separately since (3.22) fails to yield nontrivial modes. Instead of considering competition between the small spots, we instead consider competition between large and small spots collectively. We assume that $n \ge N-n$, for which $n = N-1$ is a special case, and we try to exhibit an unstable mode $\boldsymbol{c}$ of the form

$$c_1 = \ldots = c_n = c_r\,, \qquad c_{n+1} = \ldots = c_N = c_l\,. \tag{3.23}$$

Then, (3.21) reduces to the system of two equations

$$\left(B(\lambda, S_r) - \tfrac{\kappa}{1+\tau\lambda}\tfrac{n}{N}\right)c_r - \tfrac{\kappa}{1+\tau\lambda}\tfrac{(N-n)}{N}c_l = 0\,, \qquad -\tfrac{\kappa}{1+\tau\lambda}\tfrac{n}{N}c_r + \left(B(\lambda, S_l) - \tfrac{\kappa}{1+\tau\lambda}\tfrac{(N-n)}{N}\right)c_l = 0\,,$$

which admits a nontrivial solution if and only if the determinant of this 2×2 system vanishes. Therefore, to show that this mode is unstable it suffices to prove that the zero-determinant condition, written as

$$F(\lambda) \equiv B(\lambda, S_l)B(\lambda, S_r) - \frac{\kappa}{1+\tau\lambda}\left(\frac{n}{N}B(\lambda, S_l) + \frac{(N-n)}{N}B(\lambda, S_r)\right) = 0\,, \tag{3.24}$$

has a solution $\lambda > 0$. To establish this, we first differentiate $\mu(S_r) = \mu(S_l)$ with respect to S_r to obtain the identity $\mu'(S_l)S_l'(S_r) = \mu'(S_r)$. Combining this result with $B(0, S) = \mu'(S)$ we calculate that

$$F(0) = \mu'(S_l)\left[\mu'(S_r) - \kappa\frac{(N-n)}{N}\left(\frac{n}{(N-n)} + \frac{dS_l}{dS_r}\right)\right]. \tag{3.25}$$

Using $\mu'(S_l) > 0$ and $\mu'(S_r) < 0$ together with $S_l'(S_r) > -1$ (see Figure 2b) and the assumption $n/(N-n) \ge 1$, we immediately deduce that $F(0) < 0$. Next, we let $\lambda_0 > 0$ be the dominant eigenvalue of $\mathcal{M}_0$ when $S = S_l$ (see Figure 5a) so that $B(\lambda_0, S_l) = 0$. Then, from (3.24) we obtain

$$F(\lambda_0) = -\frac{\kappa}{1+\tau\lambda_0}\frac{(N-n)}{N}B(\lambda_0, S_r)\,. \tag{3.26}$$

However, since $\mathcal{M}_0$ at $S = S_r > S_{\rm crit}$ has no positive eigenvalues (see Figure 5a), we deduce that $B(\lambda, S_r)$ is of one sign for $\lambda \ge 0$ and, furthermore, it must be negative since $B(0, S_r) = \mu'(S_r) < 0$ (see Figure 5b for a plot of B showing both its continuity and negativity for all $\lambda > 0$ when $S > S_{\rm crit}$). Therefore, we have $F(\lambda_0) > 0$ and so, combined with (3.25), by the intermediate value theorem it follows that $F(\lambda) = 0$ has a positive solution. We summarize our leading order linear stability results in the following proposition:

Proposition 3.1. *(Linear Stability): Let $\varepsilon \ll 1$ and assume that $t \ll \mathcal{O}(\varepsilon^{-3})$. When $D = \mathcal{O}(1)$, the N-spot symmetric pattern from Proposition 2.1 is linearly stable. If $D = \varepsilon^{-1}D_0$ then the symmetric N-spot pattern from Proposition 2.1 is linearly stable with respect to zero-eigenvalue crossing instabilities if $\kappa < \kappa_{c1} \equiv \mu(S_{crit})/S_{crit} \approx 0.64619$ and is unstable otherwise. Moreover, it is stable with respect to Hopf instabilities on the range $\kappa > \kappa_{c1}$ if $\tau < \tau_h(\kappa)$ where $\tau_h(\kappa)$ is plotted in Figure 6a. Finally, every asymmetric N-spot pattern in the $D = \varepsilon^{-1}D_0$ regime is always linearly unstable.*

4. Slow Spot Dynamics. A wide variety of singularly perturbed RD systems are known to exhibit slow dynamics of multi-spot solutions in 2-D domains (cf. [9], [3], [13], [17]). In this section we derive a system of ODE's which characterize the motion of the spot locations $x_1, \ldots, x_N$ for the 3-D GM model on a slow time scale. Since the only N-spot patterns that may be stable on an $\mathcal{O}(1)$ time scale are (to leading order) symmetric we find that the ODE system reduces to a gradient flow. We remark that both the derivation and final ODE system are closely related to those in [16] for the 3-D Schnakenberg model.

The derivation of slow spot dynamics hinges on establishing a solvability condition for higher order terms in the asymptotic expansion in the inner region near each spot. As a result, we begin by collecting higher order expansions of the limiting behaviour as $|x - x_i| \to 0$ of the Green's functions $G(x, x_j)$ and $G_0(x, x_j)$ that satisfy (2.7) and (2.10), respectively. In particular, we calculate that

$$G(x_i + \varepsilon y, x_j) \sim \begin{cases} G(x_i, x_j) + \varepsilon y \cdot \nabla_1 G(x_i, x_j)\,, & i \neq j\,, \\ \frac{1}{4\pi\varepsilon\rho} + R(x_i) + \varepsilon y \cdot \nabla_1 R(x_i; x_i)\,, & i = j\,, \end{cases} \qquad \text{as} \quad |x - x_i| \to 0\,, \tag{4.1a}$$

where $\rho = |y|$ and $\nabla_1 R(x_i; x_i) \equiv \nabla_x R(x; x_1)|_{x=x_1}$. Likewise, for the Neumann Green's function, we have

$$G_0(x_i + \varepsilon y, x_j) \sim \frac{D_0}{\varepsilon|\Omega|} + \begin{cases} G_0(x_i, x_j) + \varepsilon y \cdot \nabla_1 G_0(x_i, x_j)\,, & i \neq j\,, \\ \frac{1}{4\pi\varepsilon\rho} + R_0(x_i) + \varepsilon y \cdot \nabla_1 R_0(x_i; x_i)\,, & i = j\,, \end{cases} \qquad \text{as} \quad |x - x_i| \to 0\,, \tag{4.1b}$$

where ∇_1 again denotes the gradient with respect to the first argument. We next extend the asymptotic construction of quasi-equilibrium patterns in §2 by allowing the spot locations to vary on a slow time scale. In particular, a dominant balance in the asymptotic expansion requires that $x_i = x_i(\sigma)$ where $\sigma = \varepsilon^3 t$. For x near x_i we introduce the two term inner expansion

$$v \sim DV_i \sim D(V_{i\varepsilon}(\rho) + \varepsilon^2 V_{i2}(y) + \cdots)\,, \qquad u \sim DU_i \sim D\big(U_{i\varepsilon}(\rho) + \varepsilon^2 U_{i2}(y) + \cdots\big)\,, \tag{4.2}$$

where we note the leading order terms are $V_{i\varepsilon}(\rho) \equiv V(\rho, S_{i\varepsilon})$ and $U_{i\varepsilon}(\rho) \equiv U(\rho, S_{i\varepsilon})$. By using the chain rule we calculate $\partial_t V_i = -\varepsilon^2 x_i'(\sigma) \cdot \nabla_y V_i$ and $\partial_t U_i = -\varepsilon^2 x_i'(\sigma) \cdot \nabla_y U_i$. In this way, upon substituting (4.2) into (1.1) we collect the $\mathcal{O}(\varepsilon^2)$ terms to obtain that V_{i2} and U_{i2} satisfy

$$\mathscr{L}_{i\varepsilon} \boldsymbol{W}_{i2} \equiv \Delta_y \boldsymbol{W}_{i2} + \mathcal{Q}_{i\varepsilon} \boldsymbol{W}_{i2} = -\boldsymbol{f}_{i\varepsilon}\,, \qquad y \in \mathbb{R}^2\,, \tag{4.3a}$$

where

$$\boldsymbol{W}_{i2} \equiv \begin{pmatrix} V_{i2} \\ U_{i2} \end{pmatrix}\,, \qquad \boldsymbol{f}_{i\varepsilon} \equiv \begin{pmatrix} \rho^{-1} V_{i\varepsilon}'(\rho)\, x_i'(\sigma) \cdot y \\ -D^{-1} U_{i\varepsilon} \end{pmatrix}\,, \qquad \mathcal{Q}_{i\varepsilon} \equiv \begin{pmatrix} -1 + 2U_{i\varepsilon}^{-1} V_{i\varepsilon} & -U_{i\varepsilon}^{-2} V_{i\varepsilon}^2 \\ 2V_{i\varepsilon} & 0 \end{pmatrix}\,. \tag{4.3b}$$

It remains to determine the appropriate limiting behaviour as $\rho \to \infty$. From the first row of $\mathcal{Q}_{i\varepsilon}$, we conclude that $V_{i2} \to 0$ exponentially as $\rho \to \infty$. However, the limiting behaviour of U_{i2} must be established by matching with the outer solution. To perform this matching, we first use the distributional limit

$$\varepsilon^{-2} v^2 \longrightarrow 4\pi\varepsilon D^2 \sum_{j=1}^N S_{j\varepsilon} \delta(x - x_j) + 2\varepsilon^3 D^2 \sum_{j=1}^N \left(\int_{\mathbb{R}^3} V_{j\varepsilon} V_{j2}\, dy \right) \delta(x - x_j)\,,$$

where the localization at each $x_1, \ldots, x_N$ eliminates all cross terms. We then update (2.8) to include the $\mathcal{O}(\varepsilon^3)$ correction term. This leads to the refined approximation for the outer solution

$$u \sim 4\pi\varepsilon D \sum_{j=1}^N S_{j\varepsilon} G(x; x_j) + 2\varepsilon^3 D \sum_{j=1}^N \left(\int_{\mathbb{R}^3} V_{j\varepsilon} V_{j2}\, dy \right) G(x; x_j)\,. \tag{4.4}$$

We observe that the leading order matching condition is immediately satisfied in both the $D = \mathcal{O}(1)$ and the $D = D_0/\varepsilon$ regimes. To establish the higher order matching condition we distinguish between the $D = \mathcal{O}(1)$ and $D = \varepsilon^{-1}D_0$ regimes and use the higher order expansions of the Green's functions as given by (4.1a) and (4.1b). In this way, in the $D = \mathcal{O}(1)$ regime we obtain the far-field behaviour as $|y| \to \infty$ given by

$$U_{i2} \sim \frac{1}{2\pi\rho}\int_{\mathbb{R}^3} V_{i\varepsilon}V_{i2}\,dy + y\cdot b_{i\varepsilon}\,, \quad \frac{b_{i\varepsilon}}{4\pi} \equiv S_{i\varepsilon}\nabla_1 R(x_i;x_i) + \sum_{j\neq i} S_{j\varepsilon}\nabla_1 G(x_i,x_j)\,. \tag{4.5}$$

Similarly, in the $D = D_0/\varepsilon$ regime we obtain the following far-field matching condition as $|y| \to \infty$:

$$U_{i2} \sim \frac{1}{2\pi\rho}\int_{\mathbb{R}^3} V_{i\varepsilon}V_{i2}\,dy + \frac{2D_0}{|\Omega|}\sum_{j=1}^{N}\int_{\mathbb{R}^3} V_{j\varepsilon}V_{j2}\,dy + y\cdot b_{0i\varepsilon}\,, \quad \frac{b_{0i\varepsilon}}{4\pi} \equiv S_{i\varepsilon}\nabla_1 R_0(x_i;x_i) + \sum_{j\neq i} S_{j\varepsilon}\nabla_1 G_0(x_i,x_j)\,. \tag{4.6}$$

In both cases, our calculations below will show that only $b_{i\varepsilon}$ and $b_{0i\varepsilon}$ affect the slow spot dynamics.

To characterize slow spot dynamics we calculate $x_i'(\sigma)$ by formulating an appropriate solvability condition. We observe for each $k = 1, 2, 3$ that the functions $\partial_{y_k}\boldsymbol{W}_{i\varepsilon}$ where $\boldsymbol{W}_{i\varepsilon} \equiv (V_{i\varepsilon}, U_{i\varepsilon})^T$ satisfy the homogeneous problem $\mathscr{L}_{i\varepsilon}\partial_{y_k}\boldsymbol{W}_{i\varepsilon} = 0$. Therefore, the null-space of the adjoint operator $\mathscr{L}_{i\varepsilon}^{\star}$ is at least three-dimensional. Assuming it is exactly three dimensional we consider the three linearly independent solutions $\boldsymbol{\Psi}_{ik} \equiv y_k\boldsymbol{P}_i(\rho)/\rho$ to the homogeneous adjoint problem, where each $\boldsymbol{P}_i(\rho) = (P_{i1}(\rho), P_{i2}(\rho)^T$ solves

$$\Delta_\rho \boldsymbol{P}_i - \frac{2}{\rho^2}\boldsymbol{P}_i + \mathcal{Q}_{i\varepsilon}^T\boldsymbol{P}_i = 0\,, \quad \rho > 0\,; \quad \boldsymbol{P}_i'(0) = \begin{pmatrix}0\\0\end{pmatrix}\,; \quad \text{with} \quad \mathcal{Q}_{i\varepsilon}^T \longrightarrow \begin{pmatrix}-1 & 0\\ 0 & 0\end{pmatrix} \quad \text{as } \rho\to\infty\,. \tag{4.7}$$

Owing to this limiting far-field behavior of the matrix $\mathcal{Q}_{i\varepsilon}^T$, we immediately deduce that $P_{i2} = \mathcal{O}(\rho^{-2})$ and that P_{i1} decays exponentially to zero as $\rho \to \infty$. Enforcing, for convenience, the point normalization condition $P_{i2} \sim \rho^{-2}$ as $\rho \to \infty$, we find that (4.7) admits a unique solution. We use each $\boldsymbol{\Psi}_{ik}$ to impose a solvability condition by multiplying (4.3a) by $\boldsymbol{\Psi}_{ik}^T$ and integrating over the ball, B_{ρ_0}, centered at the origin and of radius ρ_0 with $\rho_0 \gg 1$. Then, by using the divergence theorem, we calculate

$$\lim_{\rho_0\to\infty}\int_{B_{\rho_0}}\left(\boldsymbol{\Psi}_{ik}^T\mathscr{L}_i\boldsymbol{W}_{i2} - \boldsymbol{W}_{i2}\,\mathscr{L}_i^{\star}\boldsymbol{\Psi}_{ik}\right)dy = \lim_{\rho_0\to\infty}\int_{\partial B_{\rho_0}}\left(\boldsymbol{\Psi}_{ik}^T\partial_\rho\boldsymbol{W}_{i2} - \boldsymbol{W}_{i2}^T\partial_\rho\boldsymbol{\Psi}_{ik}\right)\Big|_{\rho=\rho_0}\rho_0^2\,d\Theta\,, \tag{4.8}$$

where Θ denotes the solid angle for the unit sphere.

To proceed, we use the following simple identities given in terms of the Kronecker symbol δ_{kl}:

$$\int_{B_{\rho_0}} y_k f(\rho)\,dy = 0\,, \qquad \int_{B_{\rho_0}} y_k y_l f(\rho)\,dy = \delta_{kl}\frac{4\pi}{3}\int_0^{\rho_0}\rho^4 f(\rho)\,d\rho\,, \qquad \text{for} \quad l,k = 1,2,3\,. \tag{4.9}$$

Since $\mathscr{L}_i^{\star}\boldsymbol{\Psi}_{ik} = 0$, we can use (4.3a) and (4.9) to calculate the left-hand side of (4.8) as

$$\begin{aligned}\lim_{\rho_0\to\infty}\int_{B_{\rho_0}}\boldsymbol{\Psi}_{ik}^T\mathscr{L}_i\boldsymbol{W}_{i2}dy &= \lim_{\rho_0\to\infty}\left(-\sum_{l=1}^{3}x_{il}'(\sigma)\int_{B_{\rho_0}} y_k y_l\frac{P_{i1}(\rho)V_{i\varepsilon}'(\rho)}{\rho^2}\,dy + \frac{1}{D}\int_{B_{\rho_0}} y_k\frac{P_{i2}(\rho)U_{i\varepsilon}(\rho)}{\rho}\,dy\right)\\ &= -\frac{4\pi}{3}x_{ik}'(\sigma)\int_0^{\infty}P_{i1}(\rho)V_{i\varepsilon}'(\rho)\rho^2\,d\rho\,.\end{aligned} \tag{4.10}$$

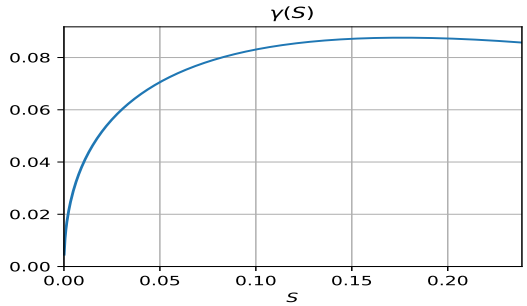

Figure 7: Plot of the numerically-computed multiplier $\gamma(S)$ as defined in the slow gradient flow dynamics (4.14).

Next, in calculating the right-hand side of (4.8) by using the far-field behavior (4.5) and (4.6), we observe that only $b_{i\varepsilon}$ and $b_{0i\varepsilon}$ terms play a role in the limit. In particular, in the $D = \mathcal{O}(1)$ regime we calculate in terms of the components of $b_{i\varepsilon l}$ of the vector $b_{i\varepsilon}$, as given in (4.5), that

$$\lim_{\rho_0\to\infty}\int_{\partial B_{\rho_0}} \boldsymbol{\Psi}_{ik}^T\partial_\rho \boldsymbol{W}_{i2}\big|_{\rho=\rho_0}\rho_0^2\,d\Theta = \lim_{\rho_0\to\infty}\sum_{l=1}^{3} b_{i\varepsilon l}\int_{\partial B_{\rho_0}}\frac{y_k y_l}{\rho_0^2}\,d\Theta = \frac{4\pi}{3}b_{i\varepsilon k}\,,$$
$$\lim_{\rho_0\to\infty}\int_{\partial B_{\rho_0}} \boldsymbol{W}_{i2}^T\partial_\rho \boldsymbol{\Psi}_{ik}\big|_{\rho=\rho_0}\rho_0^2\,d\Theta = -2\lim_{\rho_0\to\infty}\sum_{l=1}^{3} b_{i\varepsilon l}\int_{\partial B_{\rho_0}}\frac{y_k y_l}{\rho_0^2}\,d\Theta = -\frac{8\pi}{3}b_{i\varepsilon k}\,. \tag{4.11}$$

¿From (4.8), (4.10), and (4.11), we conclude for the $D = \mathcal{O}(1)$ regime that

$$x_{ik}'(\sigma) = -\frac{3}{\gamma(S_{i\varepsilon})}\,b_{i\varepsilon k}\,, \qquad \text{where} \qquad \gamma(S_{i\varepsilon}) \equiv \int_0^\infty P_{i1}(\rho)V_i'(\rho,S_{i\varepsilon})\rho^2\,d\rho\,, \tag{4.12}$$

which holds for each component $k = 1, 2, 3$ and each spot $i = 1, \ldots, N$. From symmetry considerations we see that the constant contribution to the far-field behaviour, as given by the first term in (4.5), is eliminated when integrated over the boundary. In an identical way, we can determine x_{ik}' for the $D = D_0/\epsilon$ regime. In summary, in terms of the gradients of the Green's functions and $\gamma_{i\varepsilon} \equiv \gamma(S_{i\varepsilon})$, as defined in (4.12), we obtain the following vector-valued ODE systems for the two distinguished ranges of D:

$$\frac{dx_i}{d\sigma} = -\frac{12\pi}{\gamma_{i\varepsilon}}\begin{cases}\left(S_{i\varepsilon}\nabla_1 R(x_i;x_i) + \sum_{j\neq i} S_{j\varepsilon}\nabla_1 G(x_i,x_j)\right), & \text{for } D = \mathcal{O}(1)\,,\\ \left(S_{i\varepsilon}\nabla_1 R_0(x_i;x_i) + \sum_{j\neq i} S_{j\varepsilon}\nabla_1 G_0(x_i,x_j)\right), & \text{for } D = D_0/\varepsilon\,.\end{cases} \tag{4.13}$$

Since only the symmetric N-spot configurations can be stable on an $\mathcal{O}(1)$ time scale (see Proposition 3.1), it suffices to consider the ODE systems in (4.13) when $S_{i\varepsilon} = S_\star + \mathcal{O}(\varepsilon)$ in the $D = \mathcal{O}(1)$ regime and when $S_{i\varepsilon} = S_c + \mathcal{O}(\varepsilon)$, where S_c solves (2.17), in the $D = \varepsilon^{-1}D_0$ regime. In particular, we find that to leading order, where the $\mathcal{O}(\varepsilon)$ corrections to the source strengths are neglected, the ODE systems in (4.13) can be reduced to the gradient flow dynamics

$$\frac{dx_i}{d\sigma} = -\frac{6\pi S}{\gamma(S)}\nabla_{x_i}\mathscr{H}(x_1,\ldots,x_N)\,, \qquad \text{with} \quad \gamma(S) = \int_0^\infty P_1(\rho)V_1(\rho,S)\rho^2\,d\rho\,, \tag{4.14a}$$

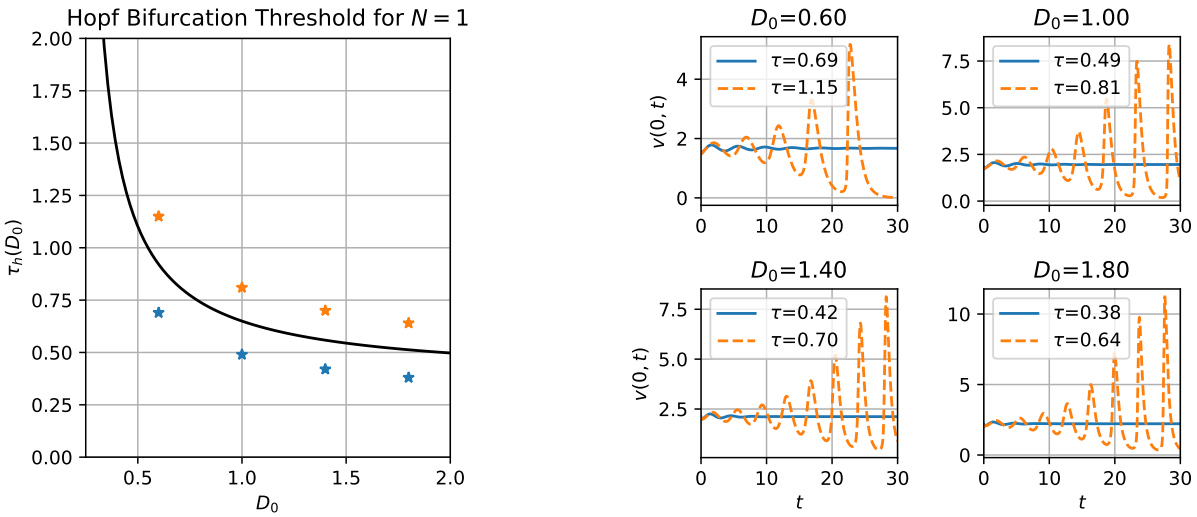

(a) (b)

Figure 8: (a) Leading order Hopf bifurcation threshold for a one-spot pattern. (b) Plots of the spot height $v(0,t)$ from numerically solving (1.1) using FlexPDE6 [6] in the unit ball with $\varepsilon = 0.05$ at the indicated τ and D_0 values.

where $S = S_\star$ or $S = S_c$ depending on whether $D = \mathcal{O}(1)$ or $D = \varepsilon^{-1} D_0$, respectively. In (4.14) the discrete energy $\mathscr{H}$, which depends on the instantaneous spot locations, is defined by

$$\mathscr{H}(x_1, \ldots, x_N) \equiv \begin{cases} \sum_{i=1}^N R(x_i) + 2\sum_{i=1}^N \sum_{j>i} G(x_i, x_j)\,, & \text{for} \quad D = \mathcal{O}(1)\,, \\ \sum_{i=1}^N R_0(x_i) + 2\sum_{i=1}^N \sum_{j>i} G_0(x_i, x_j)\,, & \text{for} \quad D = \varepsilon^{-1} D_0\,. \end{cases} \tag{4.14b}$$

In accounting for the factor of two between (4.14) and (4.13), we used the reciprocity relations for the Green's functions. In this leading order ODE system, the integral $\gamma(S)$ is the same for each spot, since $P_1(\rho)$ is computed numerically from the homogeneous adjoint problem (4.7) using the core solution $V_1(\rho, S)$ and $U_1(\rho, S)$ to calculate the matrix $\mathcal{Q}_{i\varepsilon}^T$ in (4.7). In Figure 7 we plot the numerically-computed $\gamma(S)$, where we note that $\gamma(S) > 0$. Since $\gamma(S) > 0$, local minima of $\mathscr{H}$ are linearly stable equilibria for (4.14).

We remark that this gradient flow system (4.14) differs from that derived in [16] for the 3-D Schnakenberg model only through the constant $\gamma(S)$. Since this parameter affects only the time-scale of the slow dynamics we deduce that the equilibrium configurations and stability properties for the ODE dynamics will be identical to those of the Schnakenberg model. As such, we do not analyze (4.14) further and instead refer to [16] for more detailed numerical investigations. Finally we note that the methods employed here and in [16] should be applicable to other 3-D RD systems yielding similar limiting ODE systems for slow spot dynamics. The similarity between slow dynamics for a variety of RD systems in 2-D has been previously observed and a general asymptotic framework has been pursued in [13] for the dynamics on the sphere.

5. Numerical Examples.

In this section we use FlexPDE6 [6] to numerically solve (1.1) when Ω is the unit ball. In particular, we illustrate the emergence of Hopf and competition instabilities, as predicted in §3 for symmetric spot patterns in the $D = D_0/\varepsilon$ regimes.

We begin by considering a single spot centered at the origin in the unit ball, for the $D = \varepsilon^{-1} D_0$ regime. Since no competition instabilities occur for a single spot solution, we focus exclusively on the onset of Hopf

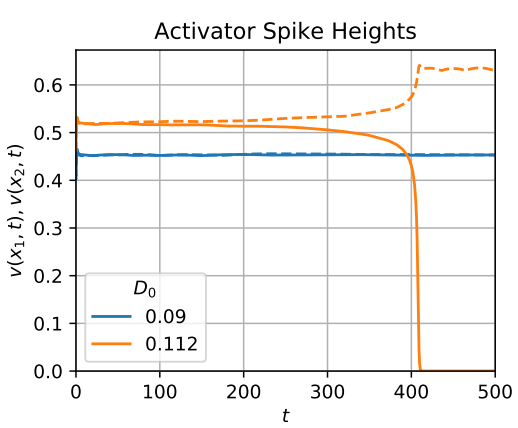

(a)

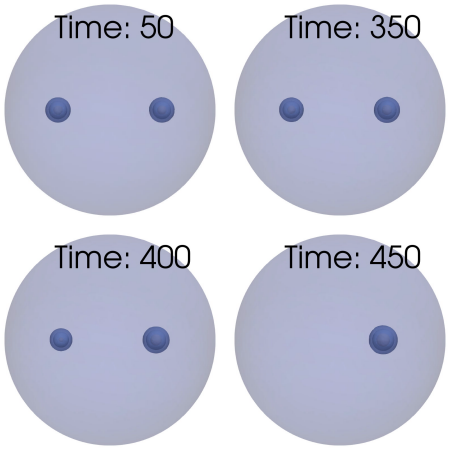

(b)

Figure 9: (a) Plots of the spot heights (solid and dashed lines) in a two-spot symmetric pattern at the indicated values of D_0. Results were obtained by using FlexPDE6 [6] to solve (1.1) in the unit ball with $\varepsilon = 0.05$ and $\tau = 0.2$. (b) plot of three-dimensional contours of $v(x,t)$ for $D_0 = 0.112$, with contours chosen at $v = 0.1, 0.2, 0.4$.

instabilities as τ is increased. In Figure 8a we plot the Hopf bifurcation threshold obtained from our linear stability theory, and indicate several sample points below and above the threshold. Using FlexPDE6 [6], we performed full numerical simulations of (1.1) in the unit ball with $\varepsilon = 0.05$ and parameters D_0 and τ corresponding to the labeled points in Figure 8a. The resulting activator height at the origin, $v(0,t)$, computed from FlexPDE6 is shown in Figure 8b for these indicated parameter values. We observe that there is good agreement with the onset of Hopf bifurcations as predicted by our linear stability theory.

Next, we illustrate the onset of a competition instability by considering a symmetric two-spot configurations with spots centered at $(\pm 0.51565, 0, 0)$ in the unit ball and with $\tau = 0.2$ (chosen small enough to avoid Hopf bifurcations) and $\varepsilon = 0.05$. The critical value of $\kappa_{c1} \approx 0.64619$ then implies that the leading order competition instability threshold for the unit ball with $|\Omega| = 4\pi/3$ is $D_0 \approx 0.64619/(3N) = 0.108$. We performed full numerical simulations of (1.1) using FlexPDE6 [6] with values of $D_0 = 0.09$ and $D_0 = 0.112$. The results of our numerical simulations are shown in Figure 9, where we observe that a competition instability occurs for $D_0 = 0.112$, as predicted by the linear stability theory. Moreover, in agreement with previous studies of competition instabilities (cf. [16], [3]), we observe that a competition instability triggers a nonlinear event leading to the annihilation of one spot.

6. The Weak Interaction Limit $D = \mathcal{O}(\varepsilon^2)$. In §3 we have shown in both the $D = \mathcal{O}(1)$ and $D = \mathcal{O}(\varepsilon^{-1})$ regimes that N-spot quasi-equilibria are not susceptible to locally non-radially symmetric instabilities. Here we consider the weak-interaction regime $D = D_0\varepsilon^2$, where we numerically determine that locally non-radially symmetric instabilities of a localized spot are possible. First, we let $\xi \in \Omega$ satisfy $\text{dist}(\xi, \partial\Omega) \gg \mathcal{O}(\varepsilon^2)$ and we introduce the local coordinates $x = \xi + \varepsilon y$ and the inner variables $v \sim \varepsilon^2 V(\rho)$ and $u \sim \varepsilon^2 U(\rho)$. With this scaling, and with $D = D_0\varepsilon^2$, the steady-state problem for (1.1) becomes

$$\Delta_\rho V - V + U^{-1}V^2 = 0\,, \qquad D_0\Delta_\rho U - U + V^2 = 0\,, \qquad \rho = |y| > 0\,. \tag{6.1}$$

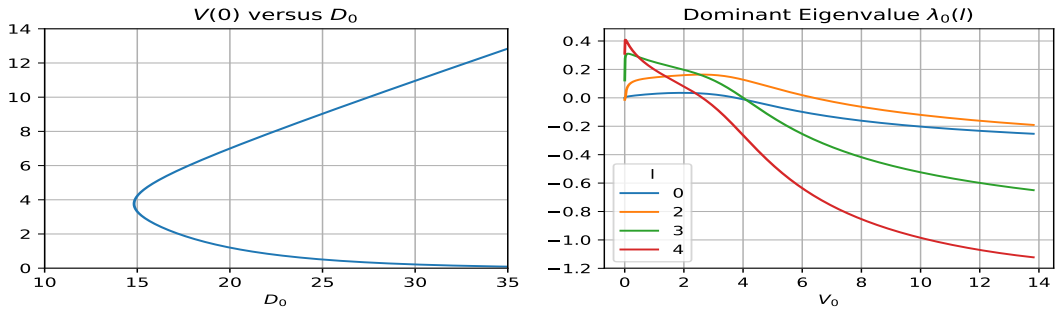

(a) (b)

Figure 10: (a) Bifurcation diagram for solutions to the core problem (6.1) in the $D = \varepsilon^2 D_0$ regime. (b) Dominant eigenvalue of the linearization of the core problem for each mode $l = 0, 2, 3, 4$, as computed numerically from (6.5).

For this core problem, we impose the boundary conditions $V_\rho(0) = U_\rho(0) = 0$ and $(V, U) \to 0$ exponentially as $\rho \to \infty$. Unlike the $D = \mathcal{O}(1)$ and $D = \mathcal{O}(\varepsilon^{-1})$ regimes, u and v are both exponentially small in the outer region. Therefore, for any well-separated configuration $x_1, \ldots, x_N$, the inner problems near each spot centre are essentially identical and independent. In Figure 10a we plot $V(0)$ versus D_0 obtained by numerically solving (6.1). From this figure, we observe that for all $D_0 \gtrapprox 14.825$, corresponding to a saddle-node point, the core problem (6.1) admits two distinct radially-symmetric solutions.

Since both the activator V and inhibitor U decay exponentially there are only exponentially weak interactions between individual spots. As a result, it suffices to consider only the linear stability of the core problem (6.1). Upon linearizing (1.1) about the core solution we obtain the eigenvalue problem

$$\Delta_\rho \Phi - \frac{l(l+1)}{\rho^2}\Phi - \Phi + \frac{2V}{U}\Phi - \frac{V^2}{U^2}\Psi = \lambda \Phi\,, \qquad D_0 \Delta_\rho \Psi - \frac{l(l+1)}{\rho^2}\Psi - \Psi + 2V\Phi = 0\,, \tag{6.2}$$

for each $l \geq 0$ and for which we impose that $\Phi'(0) = \Psi'(0) = 0$ and $(\Phi, \Psi) \to 0$ exponentially as $\rho \to \infty$. We reduce (6.2) to a single nonlocal equation by noting that the Green's function $G_l(\rho, \rho_0)$ satisfying

$$D_0 \Delta_\rho G_l - \frac{l(l+1)}{\rho^2} G_l - G_l = -\frac{\delta(\rho - \rho_0)}{\rho^2}\,, \tag{6.3}$$

is given explicitly by

$$G_l(\rho, \rho_0) = \frac{1}{D_0\sqrt{\rho_0 \rho}} \begin{cases} I_{l+1/2}(\rho/\sqrt{D_0}) K_{l+1/2}(\rho_0/\sqrt{D_0})\,, & \rho < \rho_0\,, \\ I_{l+1/2}(\rho_0/\sqrt{D_0}) K_{l+1/2}(\rho/\sqrt{D_0})\,, & \rho > \rho_0\,, \end{cases} \tag{6.4}$$

where $I_n(\cdot)$ and $K_n(\cdot)$ are the n^{th} order modified Bessel Functions of the first and second kind, respectively. As a result, by proceeding as in §3 we reduce (6.2) to the nonlocal spectral problem $\mathcal{M}_l \Phi = \lambda \Phi$ where

$$\mathcal{M}_l \Phi \equiv \Delta_\rho \Phi - \frac{l(l+1)}{\rho^2}\Phi - \Phi + \frac{2V}{U}\Phi - \frac{2V^2}{U^2}\int_0^\infty G_l(\rho, \tilde{\rho})\, V(\tilde{\rho})\, \Phi(\tilde{\rho}) \tilde{\rho}^2\, d\tilde{\rho}\,. \tag{6.5}$$

In Figure 10b we plot the real part of the largest numerically-computed eigenvalue of $\mathcal{M}_l$ as a function of $V(0)$ for $l = 0, 2, 3, 4$. From this figure, we observe that the entire lower solution branch in the $V(0)$ versus

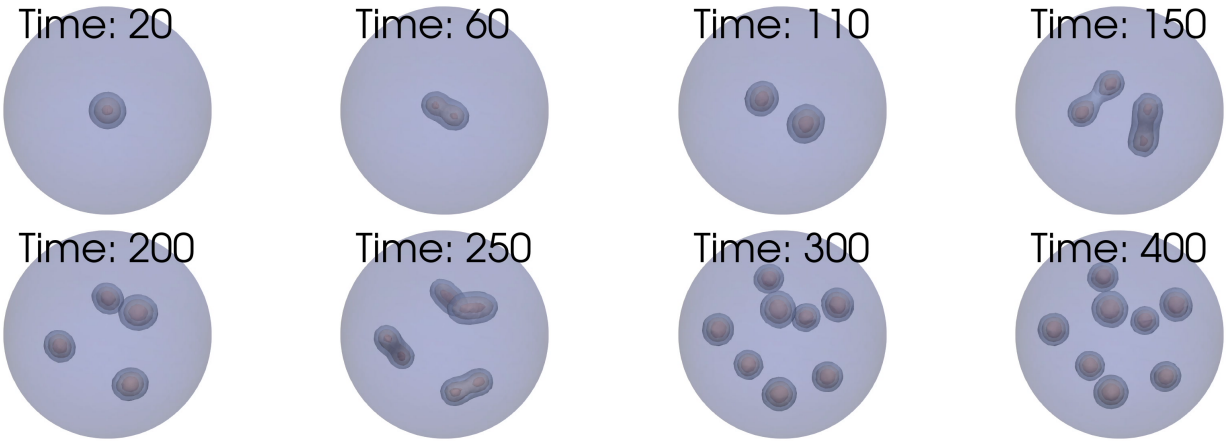

Figure 11: Snapshots of FlexPDE6 [6] simulation of (1.1) in the unit ball with $\varepsilon = 0.05$, $D = 16\varepsilon^2$, and $\tau = 1$ and with initial condition given by a single spot solution in the weak interaction limit calculated from (6.1) with $V(0) = 5$. The snapshots show contour plots of the activator $v(x,t)$ at different times where for each spot the outermost, middle, and innermost contours correspond to values of 0.006, 0.009, and 0.012 respectively. Note that the asymptotic theory predicts a maximum peak height of $v \sim \varepsilon^2 V(0) \approx 0.0125$.

D_0 bifurcation diagram in Figure 10a is unstable. However, in contrast to the $D = \mathcal{O}(1)$ and $D = \mathcal{O}(\varepsilon^{-1})$ regimes, we observe from the orange curve in Figure 10b for the $l = 2$ mode that when $D = \varepsilon^2 D_0$ there is a range of D_0 values for which a peanut-splitting instability is the only unstable mode.

In previous studies of singularly perturbed RD systems supporting peanut-splitting instabilities it has typically been observed that such linear instabilities trigger nonlinear spot self-replication events (cf. [16], [9], [13], and [3]). Recently, in [23] it has been shown using a hybrid analytical-numerical approach that peanut-splitting instabilities are subcritical for the 2-D Schnakenberg, Gray-Scott, and Brusselator models, although the corresponding issue in a 3-D setting is still an open problem. Our numerical computations below suggest that peanut-splitting instabilities for the 3-D GM model in the $D = \varepsilon^2 D_0$ regime are also subcritical. Moreover, due to the exponentially small interaction between spots, we also hypothesize that a peanut-splitting instability triggers a cascade of spot self-replication events that will eventually pack the domain with identical spots. To explore this proposed behaviour we use FlexPDE6 [6] to numerically solve (1.1) in the unit ball with parameters $\tau = 1$, $\varepsilon = 0.05$ and $D_0 = 16\varepsilon^2$, where the initial condition is a single spot pattern given asymptotically by the solution to (6.1) with $V(0) = 5$. From the bifurcation and stability plots of Figure 10 our parameter values and initial conditions are in the range where a peanut-splitting instability occurs. In Figure 11 we plot contours of the solution $v(x,t)$ at various times. We observe that the peanut-splitting instability triggered between $t = 20$ and $t = 60$ leads to a self-replication process resulting in two identical spots at $t = 110$. The peanut-splitting instability is triggered for each of these two spots and this process repeats, leading to a packing of the domain with $N = 8$ identical spots.

7. General Gierer-Meinhardt Exponents. Next, we briefly consider the generalized GM model

$$v_t = \varepsilon^2 \Delta v - v + u^{-q} v^p\,, \quad \tau u_t = D\Delta u - u + \varepsilon^{-2} u^{-s} v^m\,, \quad x \in \Omega\,; \quad \partial_n v = \partial_n u = 0\,, \quad x \in \partial\Omega\,, \tag{7.1}$$

where the GM exponents (p, q, m, s) satisfy the usual conditions $p > 1$, $q > 0$, $m > 1$, $s \geq 0$, and $\zeta \equiv mq/(p-1) - (s+1) > 0$ (cf. [19]). Although this general exponent set leads to some quantitative

differences as compared to the prototypical set $(p,q,m,s)=(2,1,2,0)$ considered in this paper, many of the qualitative properties resulting from the properties of $\mu(S)$ in Conjecture 2.1, such as the existence of symmetric quasi-equilibrium spot patterns in the $D=\mathcal{O}(1)$ regime, remain unchanged.

Suppose that (7.1) has an N-spot quasi-equilibrium solution with well-separated spots. Near the $i^{\rm th}$ spot we introduce the inner expansion $v\sim D^{\alpha}V_i(y)$, $u\sim D^{\beta}U_i(y)$, and $y=\varepsilon^{-1}(x-x_i)$, where

$$\Delta V_i - V_i + D^{(p-1)\alpha-q\beta}U_i^{-q}V_i^{p}=0\,,\qquad \Delta U_i-\varepsilon^2 D^{-1}U_i=-D^{m\alpha-(s+1)\beta-1}U_i^{-s}V_i^{m}\,,\qquad y\in\mathbb{R}^3\,.$$

Choosing α and β such that $(p-1)\alpha-q\beta=0$ and $m\alpha-(s+1)\beta=1$ we obtain

$$\alpha=\nu/\zeta\,,\qquad \beta=1/\zeta\,,\qquad \nu=q/(p-1)\,,$$

with which the inner expansion takes the form $v\sim D^{\nu/\zeta}V(\rho;S_{i\varepsilon})$ and $u\sim D^{1/\zeta}U(\rho;S_{i\varepsilon})$, where $V(\rho;S)$ and $U(\rho;S)$ are radially-symmetric solutions to the *D-independent* core problem

$$\Delta_\rho V - V + U^{-q}V^{p}=0\,,\qquad \Delta_\rho U=-U^{-s}V^{m}\,,\qquad \rho>0\,, \tag{7.2a}$$

$$\partial_\rho V(0)=\partial_\rho U(0)=0\,,\qquad V\longrightarrow 0\quad\text{and}\quad U\sim\mu(S)+S/\rho\,,\qquad \rho\to\infty\,. \tag{7.2b}$$

By using the divergence theorem, we obtain the identity $S=\int_0^\infty U^{-s}V^m\rho^2\,d\rho>0$.

By solving the core problem (7.2) numerically, we now illustrate that the function $\mu(S)$ retains several of the key qualitative properties of the exponent set $(p,q,m,s)=(2,1,2,0)$ observed in §2.1, which were central to the analysis in §2 and §3. To path-follow solutions, we proceed as in §2.1 by first approximating solutions to (7.2) for $S\ll 1$. For $S\ll 1$, we use the identity $S=\int_0^\infty U^{-s}V^m\rho^2\,d\rho>0$ to motivate a small S scaling law, and from this we readily calculate that

$$V(\rho;S)\sim\left(\frac{S}{b}\right)^{\frac{\nu}{\zeta+1}}w_c(\rho)\,,\quad U(\rho;S)\sim\left(\frac{S}{b}\right)^{\frac{1}{\zeta+1}}\,,\quad \mu(S)\sim\left(\frac{S}{b}\right)^{\frac{1}{\zeta+1}}\,,\qquad b\equiv\int_0^\infty w_c^m\rho^2 d\rho\,, \tag{7.3}$$

where $w_c>0$ is the radially-symmetric solution of

$$\Delta_\rho w_c - w_c + w_c^p=0\,,\quad \rho>0\,;\qquad \partial_\rho w_c(0)=0\,,\qquad w_c\to 0\quad\text{as }\rho\to\infty\,. \tag{7.4}$$

With this approximate solution for $S\ll 1$, we proceed as in §2.1 to calculate $\mu(S)$ in (7.2) for different GM exponent sets by path-following in S. In Figure 12b we plot $\mu(S)$ when $(p,q,m,s)=(p,1,p,0)$ with $p=2,3,4$, while a similar plot is shown in Figure 12a for other typical exponent sets in [19]. For each set considered, we find that $\mu(S)$ satisfies the properties in Conjecture 2.1. Finally, to obtain the NAS for the source strengths we proceed as in §2.2 to obtain that the outer solution for the inhibitor field is given by simply replacing D with $D^{1/\zeta}$ in (2.8). Then, by using the matching condition $u\sim D^{1/\zeta}\left(\mu(S_{j\varepsilon})+S_{j\varepsilon}\varepsilon/|x-x_j|\right)$ as $x\to x_j$, for each $j=1,\dots,N$, we conclude that the NAS (2.14) still holds for a general GM exponent set provided that $\mu(S)$ is now defined by the generalized core problem (7.2).

8. Discussion. We have used the method of matched asymptotic expansions to construct and study the linear stability of N-spot quasi-equilibrium solutions to the 3-D GM model (1.1) in the limit of an asymptotically small activator diffusivity $\varepsilon\ll 1$. Our key contribution has been the identification of two distinguished regimes for the inhibitor diffusivity, the $D=\mathcal{O}(1)$ and $D=\mathcal{O}(\varepsilon^{-1})$ regimes, for which we constructed N-spot quasi-equilibrium patterns, analyzed their linear stability, and derived an ODE system

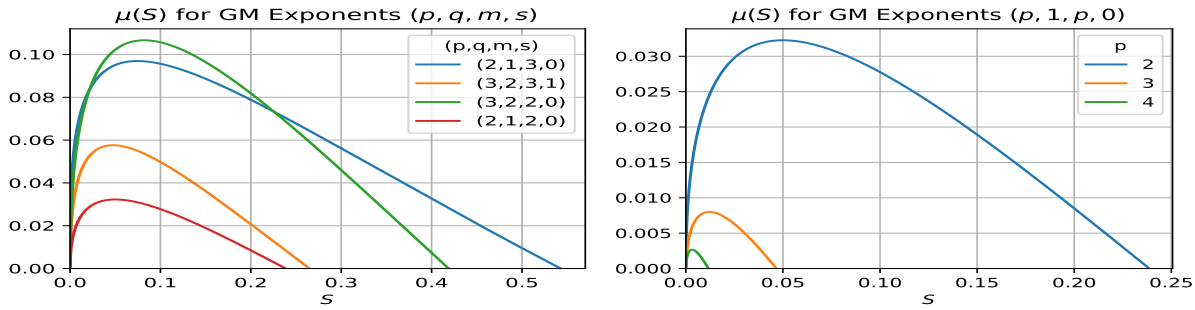

(a) (b)

Figure 12: Left panel: Plot of $\mu(S)$, computed from the generalized GM core problem (7.2), for the indicated exponent sets (p, q, m, s). Right panel: $\mu(S)$ for exponent sets $(p, 1, p, 0)$ with $p = 2, 3, 4$. For each set, there is a unique $S = S_\star$ for which $\mu(S_\star) = 0$. The properties of $\mu(S)$ in Conjecture 2.1 for the protypical set $(2, 1, 2, 0)$ still hold.

governing their slow spot dynamics. We determined that in the $D = \mathcal{O}(1)$ regime all N-spot patterns are, to leading order in ε, symmetric and linearly stable on an $\mathcal{O}(1)$ time scale. On the other hand, in the $D = \mathcal{O}(\varepsilon^{-1})$ regime we found the existence of both symmetric and asymmetric N-spot patterns. However, we demonstrated that all asymmetric patterns are unstable on an $\mathcal{O}(1)$ time scale, while for the symmetric patterns we calculated Hopf and competition instability thresholds. These GM results are related to those in [16] for the 3-D singularly perturbed Schnakenberg model, with one of the key new features being the emergence of *two* distinguished limits, and in particular the existence of localized solutions in the $D = \mathcal{O}(1)$ regime for the GM model. For $D = \mathcal{O}(1)$, concentration behavior for the Schnakenberg model as $\varepsilon \to 0$ is no longer at discrete points typical of spot patterns, but instead appears to occur on higher co-dimension structures such as thin sheets and tubes in 3-D (cf. [14]). For the GM model, we illustrated the onset of both Hopf and competition instabilities by numerically solving the full GM PDE system using the finite element software FlexPDE6 [6]. We have also considered the weak-interaction regime $D = \mathcal{O}(\varepsilon^2)$, where we used a hybrid analytical-numerical approach to calculate steady-state solutions and determine their linear stability properties. In this small D regime we found that spot patterns are susceptible to peanut-splitting instabilities. Finally, using FlexPDE6 we illustrated how the weak-interaction between spots together with the peanut-splitting instability leads to a cascade of spot self-replication events.

We conclude by highlighting directions for future work and open problems. First, although we have provided numerical evidence for the properties of $\mu(S)$ highlighted in Conjecture 2.1, a rigorous proof remains to be found. In particular, we believe that it would be significant contribution to rigorously prove the existence and uniqueness of the *ground state* solution to the core problem (2.1), which we numerically calculated when $S = S_\star$. A broader and more ambitious future direction is to characterize the reaction kinetics $F(V, U)$ and $G(V, U)$ for which the core problem

$$\Delta_\rho V + F(V, U) = 0, \qquad \Delta_\rho U + G(V, U) = 0, \qquad \text{in } \rho > 0\,, \tag{8.1}$$

admits a radially-symmetric ground state solution for which $V \to 0$ exponentially and $U = \mathcal{O}(\rho^{-1})$ as $\rho \to \infty$. The existence of such a ground state plays a key role in determining the regimes of D for which localized solutions can be constructed. For example, in the study of the 3-D singularly perturbed

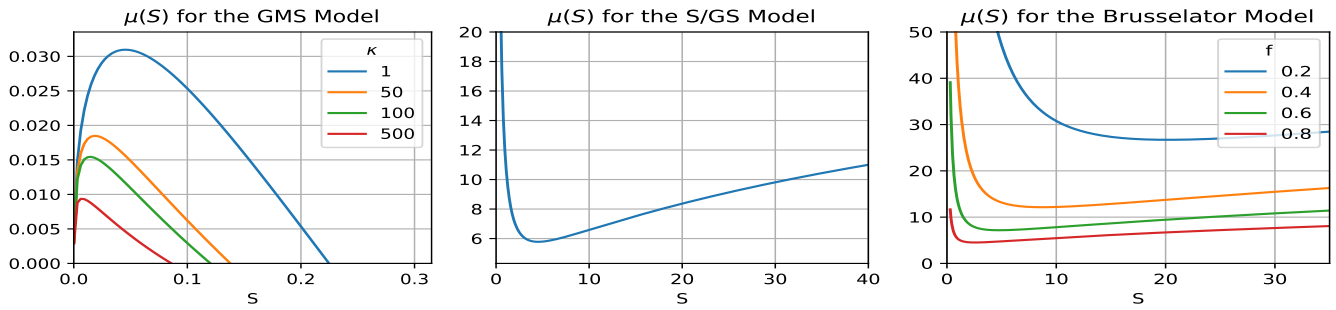

(a) (b) (c)

Figure 13: Plots of the far-field constant behaviour for the (a) Gierer-Meinhardt with saturation, (b) Schnakenberg or Gray-Scott, and (c) Brusselator models. See Table 1 for the explicit form of the kinetics $F(v,u)$ and $G(v,u)$ for each model. A zero-crossing of $\mu(S)$ at some $S>0$ occurs only for the GMS model.

Schnakenberg model it was found that the core problem does not admit such a solution and as a result localized spot solutions could not be constructed in the $D=\mathcal{O}(1)$ regime (cf. [16]). To further motivate such an investigation of (8.1) we extend our numerical method from §2.1 to calculate and plot in Figure 13 the far-field constant $\mu(S)$ for the core problems associated with the GM model with saturation (GMS), the Schnakenberg/Gray-Scott (S/GS) model, and the Brusselator (B) model (see Table 1 for more details). Note that for the GMS model we can find values of $S_\star$ such that $\mu(S_\star)=0$, but such a zero-crossing does not appear to occur for the (S/GS) and (B) models. As a consequence, for these three specific RD systems, localized spot patterns in the $D=\mathcal{O}(1)$ regime should only occur for the GMS model. Additionally, understanding how properties of $\mu(S)$, such as convexity and positiveness, are inherited from the reaction kinetics would be a significant contribution. In this direction, it would be interesting to try extend the rigorous numerics methodology of [1] to try to establish Conjecture 2.1.

Acknowledgments. Daniel Gomez was supported by an NSERC Doctoral Fellowship. Michael Ward and Juncheng Wei gratefully acknowledge the support of the NSERC Discovery Grant Program.

REFERENCES

RD Model	$F(V,U)$	$G(V,U)$	Decay behavior
Gierer-Meinhardt with Saturation (GMS)	$-V+\frac{V^2}{U(1+\kappa U^2)}$	V^2	$U\sim\mu(S)+S/\rho$
Schnakenberg or Gray-Scott (S/GS)	$-V+V^2U$	$-V^2U$	$U\sim\mu(S)-S/\rho$
Brusselator (B)	$-V+fV^2U$	$V-V^2U$	$U\sim\mu(S)-S/\rho$

Table 1: Core problems and far-field inhibitor behaviour for some common RD systems.

[1] I. Balázs, J. van den Berg, J. Courtois, J. Dudás, J. P. Lessard, A. Vörös-Kiss, J. F. Williams, and X. Y. Yin. Computer-assisted proofs for radially symmetric solutions of PDEs. *J. Comput. Dynamics*, 5(1 & 2):61–80, 2018.

[2] C. N. Chen, Y. S. Choi, Y. Hu, and X. Ren. Higher dimensional bubble profiles in a sharp interface limit of the FitzHugh-Nagumo system. *SIAM J. Math. Anal.*, 50(5):5072–5095, 2018.

[3] W. Chen and M. J. Ward. The stability and dynamics of localized spot patterns in the two-dimensional Gray-Scott model. *SIAM J. Appl. Dyn. Sys.*, 10(2):582–666, 2011.

[4] A. Doelman and H. Van der Ploeg. Homoclinic stripe patterns. *SIAM J. Appl. Dyn. Sys.*, 1(1):65–104, 2002.

[5] S. I. Ei and S. Y. Tzeng. Spike solutions for a mass conservation reaction-diffusion system. *DCDS Series A*, 40(6):3357–3374, 2020.

[6] P. FlexPDE. Solutions inc. *URL http://www. pdesolutions. com*, 2015.

[7] A. Gierer and H. Meinhardt. A theory of biological pattern formation. *Kybernetik*, 12(1):30–39, Dec 1972.

[8] T. Kolokolnikov, M. J. Ward, and J. Wei. Pulse-splitting for some reaction-diffusion systems in one-space dimension. *Studies App. Math.*, 114(2):115–165., 2005.

[9] T. Kolokolnikov, M. J. Ward, and J. Wei. Spot self-replication and dynamics for the Schnakenberg model in a two-dimensional domain. *J. Nonlinear Sci.*, 19(1):1–56, 2009.

[10] M. Leda, V. K. Vanag, and I. R. Epstein. Instabilities of a three-dimensional localized spot. *Phys. Rev. E*, 80:066204, 2009.

[11] Y. Nishiura. *Far-from Equilibrium dynamics: Translations of mathematical monographs*, volume 209. AMS Publications, Providence, Rhode Island, 2002.

[12] R. Straube and M. J. Ward. Intraceulluar signalling gradients arising from multiple compartments: A matched asymptotic expansion approach. *SIAM J. Appl. Math.*, 70(1):248–269, 2009.

[13] P. H. Trinh and M. J. Ward. The dynamics of localized spot patterns for reaction-diffusion systems on the sphere. *Nonlinearity*, 29(3):766–806, 2016.

[14] J. Tzou. private communication.

[15] J. C. Tzou, M. J. Ward, and J. C. Wei. Anomalous scaling of Hopf bifurcation thresholds for the stability of localized spot patterns for reaction-diffusion systems in two dimensions. *SIAM J. Appl. Dyn. Syst.*, 17(1):982–1022, 2018.

[16] J. C. Tzou, S. Xie, T. Kolokolnikov, and M. J. Ward. The stability and slow dynamics of localized spot patterns for the 3-D Schnakenberg reaction-diffusion model. *SIAM J. Appl. Dyn. Syst.*, 16(1):294–336, 2017.

[17] M. J. Ward. Spots, traps, and patches: Asymptotic analysis of localized solutions to some linear and nonlinear diffusive processes. *Nonlinearity*, 31(8):R189 (53), 2018.

[18] M. J. Ward and J. Wei. Asymmetric spike patterns for the one-dimensional Gierer-Meinhardt model: Equilibria and stability. *European J. Appl. Math.*, 13(3):283–320, 2002.

[19] M. J. Ward and J. Wei. Hopf bifurcation of spike solutions for the shadow Gierer-Meinhardt model. *European J. Appl. Math.*, 14(6):677–711, 2003.

[20] J. Wei. Existence and stability of spikes for the Gierer-Meinhardt system. In M. Chipot, editor, *Handbook of Differential Equations, Stationary Partial Differential Equations*, volume 5, pages 489–581. Elsevier, 2008.

[21] J. Wei and M. Winter. Spikes for the two-dimensional Gierer-Meinhardt system: The weak coupling case. *J. Nonlinear Sci.*, 11(6):415–458, 2001.

[22] J. Wei and M. Winter. *Mathematial aspects of pattern formation in biological systems*, volume 189. Applied Mathematical Sciences Series, Springer, 2014.

[23] T. Wong and M. J. Ward. Weakly nonlinear analysis of peanut-shaped deformations for localized spots of singularly perturbed reaction-diffusion systems. *to appear, SIAM J. Appl. Dyn. Sys.*, 2020.